

Global absence and targeting of protective immune states in severe COVID-19

<https://doi.org/10.1038/s41586-021-03234-7>

Received: 23 October 2020

Accepted: 12 January 2021

Published online: 25 January 2021

 Check for updates

Alexis J. Combes^{1,2,3,18}✉, Tristan Courau^{1,2,3,18}, Nicholas F. Kuhn^{1,2,18}, Kenneth H. Hu^{1,2,18}, Arja Ray^{1,2,18}, William S. Chen^{2,4}, Nayvin W. Chew^{1,2,3}, Simon J. Cleary^{2,5,6}, Divyashree Kushnoor^{1,2,3}, Gabriella C. Reeder^{1,2,3}, Alan Shen^{1,2,3}, Jessica Tsui^{1,2,3}, Kamir J. Hiam-Galvez^{2,7,8}, Priscila Muñoz-Sandoval^{2,8,9}, Wandi S. Zhu^{2,8,9}, David S. Lee^{2,10,11}, Yang Sun^{2,10,11}, Ran You^{1,2}, Méliá Magnen^{2,5,6}, Lauren Rodriguez^{2,7}, K. W. Im^{1,2,3}, Nina K. Serwas^{1,2}, Aleksandra Leligdowicz^{5,6}, Colin R. Zamecnik^{2,12}, Rita P. Loudermilk^{2,12}, Michael R. Wilson^{2,12}, Chun J. Ye^{2,10,11}, Gabriela K. Fragiadakis^{2,3,10,11}, Mark R. Looney^{2,5,6}, Vincent Chan^{1,2}, Alyssa Ward^{10,11}, Sidney Carrillo^{5,6}, The UCSF COMET Consortium*, Michael Matthay^{5,6}, David J. Erle^{2,3,5,6}, Prescott G. Woodruff^{2,5,6}, Charles Langelier¹³, Kirsten Kangelaris¹⁴, Carolyn M. Hendrickson^{5,6}, Carolyn Calfee^{5,6}, Arjun Arka Rao^{1,2,3}✉ & Matthew F. Krummel^{1,2}✉

Although infection with severe acute respiratory syndrome coronavirus 2 (SARS-CoV-2) has pleiotropic and systemic effects in some individuals^{1–3}, many others experience milder symptoms. Here, to gain a more comprehensive understanding of the distinction between severe and mild phenotypes in the pathology of coronavirus disease 2019 (COVID-19) and its origins, we performed a whole-blood-preserving single-cell analysis protocol to integrate contributions from all major immune cell types of the blood—including neutrophils, monocytes, platelets, lymphocytes and the contents of the serum. Patients with mild COVID-19 exhibit a coordinated pattern of expression of interferon-stimulated genes (ISGs)³ across every cell population, whereas these ISG-expressing cells are systemically absent in patients with severe disease. Paradoxically, individuals with severe COVID-19 produce very high titres of anti-SARS-CoV-2 antibodies and have a lower viral load compared to individuals with mild disease. Examination of the serum from patients with severe COVID-19 shows that these patients uniquely produce antibodies that functionally block the production of the ISG-expressing cells associated with mild disease, by activating conserved signalling circuits that dampen cellular responses to interferons. Overzealous antibody responses pit the immune system against itself in many patients with COVID-19, and perhaps also in individuals with other viral infections. Our findings reveal potential targets for immunotherapies in patients with severe COVID-19 to re-engage viral defence.

To better understand the biology of the immune response to SARS-CoV-2, we compared patients with COVID-19 (that is, who tested positive for the SARS-CoV-2 virus) to patients who presented with similar respiratory symptoms but who were not infected with SARS-CoV-2. We enrolled 21 in-patients who were positive for SARS-CoV-2; 11 in-patients with similar clinical presentations, consistent with acute lung injury or acute respiratory distress syndrome, who were negative for SARS-CoV-2 (that is, with their symptoms caused by other infections or of unknown origin); and 14 healthy control individuals.

We further categorized these individuals as having ‘mild–moderate’ disease (requiring short stays in hospital with no need for mechanical ventilation and intensive care) or ‘severe’ disease (requiring intubation and intensive care) according to the full clinical course of their disease (Fig. 1a, Extended Data Fig. 1a, Supplementary Table 1). Our study therefore includes patients with mild–moderate COVID-19 ($n = 11$), patients with severe COVID-19 ($n = 10$), and patients with mild–moderate ($n = 6$) or severe ($n = 5$) acute lung injury or acute respiratory distress syndrome not related to COVID-19. With the exception of one individual, all of the

¹Department of Pathology, University of California San Francisco, San Francisco, CA, USA. ²ImmunoX Initiative, University of California San Francisco, San Francisco, CA, USA. ³UCSF CoLabs, University of California San Francisco, San Francisco, CA, USA. ⁴Department of Radiation Oncology, University of California San Francisco, San Francisco, CA, USA. ⁵Division of Pulmonary and Critical Care Medicine, Department of Medicine, University of California San Francisco, San Francisco, CA, USA. ⁶Cardiovascular Research Institute, University of California San Francisco, San Francisco, CA, USA. ⁷Department of Otolaryngology, University of California San Francisco, San Francisco, CA, USA. ⁸Department of Microbiology and Immunology, University of California San Francisco, San Francisco, CA, USA. ⁹Sandler Asthma Basic Research Center, University of California San Francisco, San Francisco, CA, USA. ¹⁰Institute for Human Genetics, University of California San Francisco, San Francisco, CA, USA. ¹¹Division of Rheumatology, Department of Medicine, University of California San Francisco, San Francisco, CA, USA. ¹²Department of Neurology, Weill Institute for Neurosciences, University of California San Francisco, San Francisco, CA, USA. ¹³Division of Infectious Disease, Department of Medicine, University of California San Francisco, San Francisco, CA, USA. ¹⁴Division of Hospital Medicine, Department of Medicine, University of California San Francisco, San Francisco, CA, USA. ¹⁸These authors contributed equally: Alexis J. Combes, Tristan Courau, Nicholas F. Kuhn, Kenneth H. Hu, Arja Ray. *A list of authors and their affiliations appears at the end of the paper. ✉e-mail: Alexis.Combes@ucsf.edu; ArjunArka.Rao@ucsf.edu; Matthew.Krummel@ucsf.edu

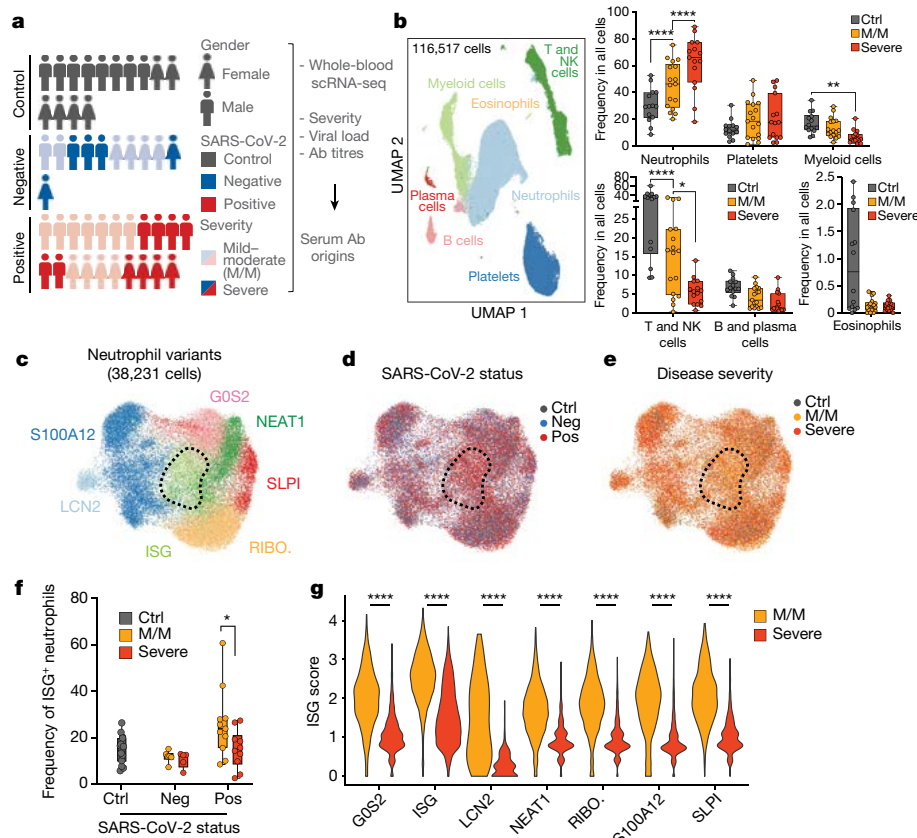


Fig. 1 | Severe COVID-19 disease is characterized by a lack of interferon-responsive neutrophils. **a**, Left, gender, SARS-CoV-2 status and disease severity in patients and healthy control individuals, Right, description of study design. Ab, antibody. **b**, Left, uniform manifold approximation and projection (UMAP) visualization of 116,517 cells merged from the entire cohort with specific populations of cells overlaid. Right, frequencies of these cell populations among healthy control individuals (Ctrl), patients with mild-moderate disease (M/M) and patients with severe disease. **c**, UMAP visualization of neutrophil subsets. The subsets are named on the basis of their gene expression; RIBO., enriched in ribosomal proteins. **d**, **e**, Overlay of

SARS-CoV-2 status and disease severity, respectively, on the neutrophil UMAP. **f**, Frequency of ISG⁺ neutrophils among all neutrophils according to SARS-CoV-2 status (positive or negative) and disease severity (control, $n = 14$; SARS-CoV-2-negative M/M, $n = 6$; SARS-CoV-2-negative severe, $n = 5$; SARS-CoV-2-positive M/M, $n = 11$; SARS-CoV-2-positive severe $n = 10$). **g**, ISG-signature score across neutrophil subtypes and disease severity in patients who were positive for SARS-CoV-2. Statistical significance was assessed using a two-way analysis of variance (ANOVA) with multiple comparisons (**a**, **e**) or a two-sided Wilcoxon test (**f**). * $P < 0.05$, ** $P < 0.01$, **** $P < 0.0001$. For box plots in **b**, **f**: centre line, median; box limits, 25th and 75th percentiles; whiskers, minimum and maximum values.

patients who presented with mild-moderate disease remained mild-moderate during hospitalization (Extended Data Fig. 1a), suggesting that mild-moderate and severe are stable states rather than transient phases of disease in this cohort.

As the majority of COVID-19 mortality occurs in patients with acute respiratory distress syndrome, which is characterized by a strong immune response with prominent contributions from neutrophils, monocytes and platelets, we focused on collecting these cells along with other major populations. We thus performed single-cell RNA sequencing (scRNA-seq) on red-blood-cell-depleted blood samples from all individuals. After merging, batch correction and doublet removal, our data comprised 116,517 cells (Fig. 1b, Extended Data Fig. 1b), among which we identified neutrophils, platelets, mononuclear phagocytes, T cells, natural killer (NK) cells, B cells, plasma cells and eosinophils (Fig. 1b, Extended Data Fig. 1c). We confirmed a positive association between neutrophil frequency and disease severity and an inverse correlation for lymphoid populations¹⁻³ (Fig. 1b, Extended Data Fig. 1d). At this level of resolution, findings were similar between individuals who were negative and those who were positive for the SARS-CoV-2 virus (Extended Data Fig. 1f-e).

Within the neutrophils, we identified seven subtypes (Fig. 1c, Extended Data Fig. 2a), consistent with previous studies²⁴. One population, expressing a strong interferon-stimulated gene (ISG) signature (hereafter termed ISG neutrophils), was highly enriched in patients

with COVID-19, but not in those whose disease was severe (Fig. 1d, e, Extended Data Fig. 2b). Separate pseudotime analysis (Extended Data Fig. 2d-g) placed the ISG subtype at a late stage of differentiation, and showed that this was the only such state that was significantly altered between patients with mild-moderate illness and those with severe illness (Extended Data Fig. 2e), and specifically within the individuals who were positive for SARS-CoV-2 (Fig. 1f, Extended Data Fig. 2c). ISG-signature genes include master antiviral regulators such as *ISG15* and *IFITM3*, the latter of which encodes interferon-induced transmembrane protein 3, which restricts viral entry into the cytosol⁵.

We also analysed differentially expressed genes (DEGs) from patients who were positive versus those who were negative for SARS-CoV-2, and from patients with mild-moderate disease versus those with severe disease, across all neutrophils. ISG-signature genes showed a higher relative level of expression in all neutrophil subtypes, specifically in patients with mild-moderate disease who were SARS-CoV-2-positive, as compared to patients with severe disease who were SARS-CoV-2-positive (Fig. 1g, Extended Data Fig. 2h-n). By contrast, a separate neutrophil-degranulation gene program was upregulated in neutrophils from patients with severe disease compared to patients with mild-moderate disease regardless of COVID-19 status (Extended Data Fig. 2o-p). This suggests that there is a shared program of degranulation enhancement in all respiratory infections regardless of the causative pathogen, and that a global induction of the ISG program

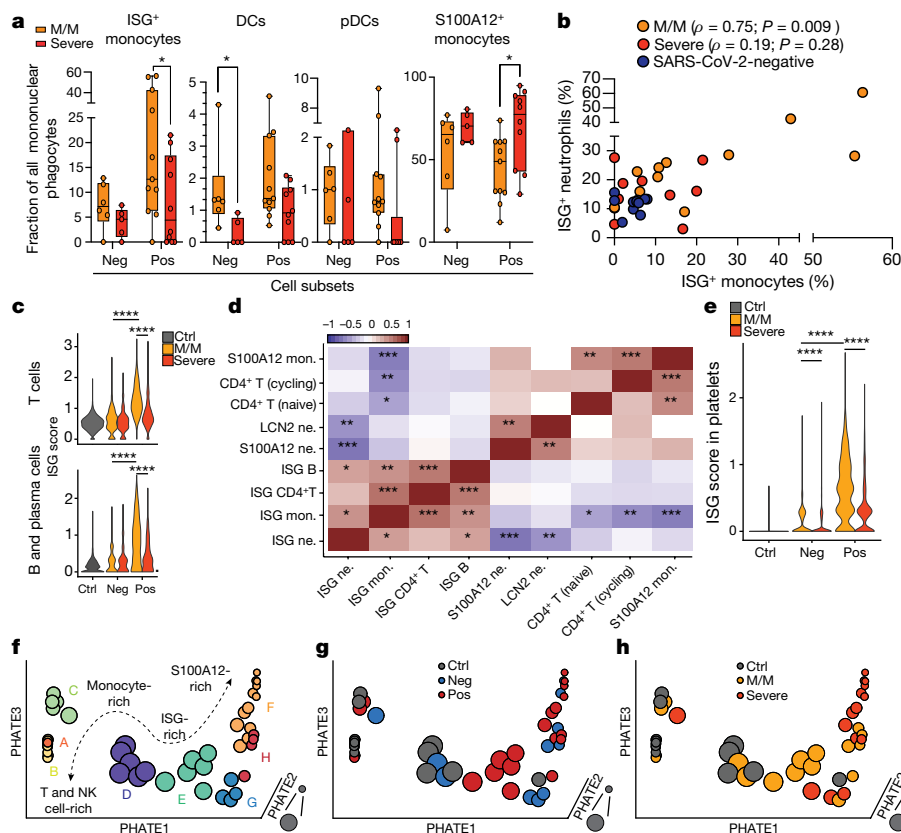


Fig. 2 | Severe COVID-19 disease is defined by the lack of a concerted interferon response across peripheral blood immune cells. a, Frequencies of mononuclear phagocyte subsets among all mononuclear phagocytes in individuals with mild–moderate disease (SARS-CoV-2-negative, $n = 6$; SARS-CoV-2-positive, $n = 11$) and severe disease (SARS-CoV-2-negative, $n = 5$; SARS-CoV-2-positive, $n = 10$). DCs, dendritic cells; pDCs, plasmacytoid dendritic cells. Centre line, median; box limits, 25th and 75th percentiles; whiskers, minimum and maximum values. **b**, Scatter plot showing the correlation between ISG⁺ neutrophil and ISG⁺ monocyte subsets in the indicated groups of patients. P values and Spearman's rank correlation coefficients (ρ) are shown (M/M, $n = 11$; severe, $n = 10$; SARS-CoV-2-negative, $n = 11$). **c**, Violin plots of ISG-signature scores in all T cells (top) and all B and plasma cells (bottom) by SARS-CoV-2 status and disease severity. Statistical

significance was assessed using a two-sided Wilcoxon test. **d**, Correlation matrix using Spearman's rank correlation between the most- and the least-correlated cell subsets to the ISG⁺ neutrophils (data include all of the patients who were negative and patients who were positive for SARS-CoV-2). Mon., monocytes; ne., neutrophils. **e**, ISG-signature score in all platelets, by SARS-CoV-2 status and disease severity. **f–h**, Three-dimensional PhEMD embedding of all patients, coloured by de novo patient clusters A–H (f), SARS-CoV-2 status (g) and disease severity (h). PHATE, potential of heat diffusion for affinity-based transition embedding. Statistical significance was assessed using a two-tailed Spearman's rank correlation test (b), a Kruskal–Wallis test with multiple comparisons (a) or a two-sided Wilcoxon test (c, e). * $P < 0.05$, **** $P < 0.0001$.

occurs in all neutrophils in patients with mild–moderate COVID-19 that is absent in patients with severe COVID-19³.

Assessment of the mononuclear phagocytes—monocytes, macrophages, dendritic cells and plasmacytoid dendritic cells—yielded seven clusters of transcriptionally distinct cell subsets, which were evenly distributed across our cohort (Extended Data Fig. 3a–f). We identified an ISG-expressing cluster of classical monocytes as being enriched in patients with COVID-19, and particularly in those with mild–moderate disease—similarly to neutrophils (Fig. 2a, Extended Data Fig. 4a–c). ISG-expressing monocytes also expressed genes associated with glycolysis; by contrast, a subset of monocytes expressing S100 calcium-binding protein A12 (S100A12) was enriched for genes associated with oxidative phosphorylation, consistent with previous reports on bacterial sepsis⁶ (Extended Data Fig. 4d). An analysis of DEGs demonstrated that ISGs were the dominant genes associated with mild–moderate phenotypes when the entire pool of mononuclear phagocytes was assessed (Extended Data Fig. 4e).

The frequencies of ISG-expressing (ISG⁺) monocytes and ISG⁺ neutrophils were strongly correlated with one another in individuals with mild–moderate COVID-19 (Fig. 2b, Extended Data Fig. 4f). A comprehensive analysis of T cell and B cell frequencies (Extended Data Fig. 5)

showed that both cell types were also significantly enriched in ISG signatures, specifically in patients with mild–moderate COVID-19 (Fig. 2c). The frequency of ISG⁺ cells in one compartment correlated with that in another compartment—for example, ISG⁺ T cells and ISG⁺ neutrophils—uniquely in patients with mild–moderate disease (Extended Data Fig. 4g). Spearman correlation analysis across multiple cell types in all patients thus showed a collection of correlated ISG⁺ populations and a second anticorrelated block of other cell populations, notably those expressing S100A12 (Fig. 2d).

Our scRNA-seq whole-blood dataset also allowed us to identify platelets and categorize them into subsets on the basis of established platelet signature genes (Fig. 1a, Extended Data Fig. 1d). Analysis of these genes found six clusters, including three (named 'H3F3B', 'HIST1H2AC' and 'RGS18') that still carried transcripts acquired from the parental cells (megakaryocytes)⁷ (Extended Data Fig. 6a, b). The HIST1H2AC subset was depleted only modestly in patients with severe COVID-19, suggesting a skewing away from 'younger' cells (Extended Data Fig. 6c). To investigate this finding further, we overlaid the expression of *BCL2L1*, which has been identified as a 'molecular clock' for platelet lifetime, onto our dataset⁸. This identified a histone-rich H3F3B cluster as representing 'young' platelets (Extended Data Fig. 6d)—a result

supported by a second signature of transcripts in young, reticulated platelets⁹ (Extended Data Fig. 6e). Pseudotime analysis rooted at this H3F3B cluster (Extended Data Fig. 6f, g) suggested again that platelets from all patients with disease were broadly overrepresented at the end of the trajectory (Extended Data Fig. 6h). Although we did not identify a distinct ISG⁺ cluster (Extended Data Fig. 6i), akin to myeloid and lymphoid cells, ISG-signature scores in platelets from patients with mild–moderate disease were increased relative to those from patients with severe disease, particularly for individuals with COVID-19 (Fig. 2e).

Platelet scRNA-seq also permitted the identification of heterotypic aggregates between platelets and nonplatelets by using a ‘platelet-first’ approach (Extended Data Fig. 7a–c). This approach revealed the presence of platelet transcripts associated with cells that also bore signatures of other major blood cell types (Extended Data Fig. 7a–c). We found no notable differences in frequencies of cell types in this ‘platelet-first’ object compared to the original dataset (Extended Data Fig. 7e). This suggests that, at least in circulating blood, platelets form aggregates indiscriminately with varying other cell types without favouring one cell type over another.

Holistic assessment of severe COVID-19

After observing that ISG expression profiles were increased in every cell type among patients with mild–moderate disease but globally reduced with severe illness, we turned to a holistic view of disease states. PhEMD (‘phenotypic earth mover’s distance’)¹⁰ embedding of patients on the basis of their cell subtype frequencies revealed eight distinct groups of patients (Fig. 2f, Extended Data Fig. 7f), in which the progression from A through to H represents patients with a generally increasing relative frequency of neutrophils. Groups C, D, G and H include patients with a relative enrichment of monocytes. Group E represents patients with an enrichment of ISG⁺ neutrophils, and mostly consists of SARS-CoV-2-positive patients with mild–moderate disease (Fig. 2g, h). By contrast, Group G, which is an alternative and ‘severe’ fate for patients, is highly enriched for neutrophils and has a predominance of S100A12⁺ rather than ISG⁺ neutrophils (Extended Data Fig. 7f).

Examination of serum interferon α (IFN α) levels could not explain the loss of ISG⁺ cell populations in patients with severe illness, as substantial levels of IFN α production were observed in some of these patients (Fig. 3a). However, ISG⁺ cell populations were strongly correlated with a lower severity of COVID-19 illness, exhibiting higher serum IFN α concentration and lower plasma levels of surfactant protein D (SP-D) (indicative of alveolar epithelial injury) (Extended Data Fig. 8a). When compared to a high-dimensional panel of plasma protein levels (Extended Data Fig. 8c), most ISG⁺ cell subtypes clustered together and correlated with factors indicative of a strong ISG and T helper 1 (T_H1) response (CXCL1, CXCL6, CXCL10, CXCL11, TNFB, IL-12B, MCP2 and MCP4). An unexpected anticorrelate of the ISG state was the concentration of serum antibodies against the SARS-CoV-2 spike and nucleocapsid proteins (Fig. 3b, Extended Data Fig. 8a).

This anticorrelation was marked, and was not strongly mirrored in higher total levels of IgG antibodies or immune complexes in sera from patients with severe COVID-19 (Extended Data Fig. 8d–f). We considered it a paradox that patients with severe COVID-19 had higher levels of potentially neutralizing antibodies. This finding appears to contradict previous reports showing that viral load is associated with severity and mortality in COVID-19^{11,12}—a difference which could be explained by the fact that these studies examined patients with high mortality, which was a very rare event in our cohort (Supplementary Table 1). At the day of admission, the specificities of both antibodies (that is, against the SARS-CoV-2 spike and nucleocapsid proteins) were anticorrelated with the viral load as assessed from nasal swabs (Fig. 3c, Extended Data Fig. 8b), consistent with (though not definitive evidence for) these being neutralizing antibodies. As increased antibody titres and decreased viral load have been reported to be a feature of later

stages of disease¹³, we considered the hypothesis that our observed mild–moderate disease simply preceded severe disease. However, we found that antibody titres in patients with severe COVID-19 were consistently higher compared to patients with mild–moderate disease over time—even two weeks after the onset of symptoms (Fig. 3d, Extended Data Fig. 8e)—and only 1 of our 21 patients with mild–moderate disease went on to develop severe disease (Extended Data Fig. 1b). Finally, we observed no statistical correlation between the day of onset of symptoms and the presence of ISG⁺ cell populations (Extended Data Fig. 8a). These elements would seem to argue against a simple temporal relationship between mild–moderate and severe states, and led us to investigate a systemic aetiology for this split in states in the serum.

Antibodies antagonize the ISG response

Considering this enhancement of antibodies, we first asked whether serum from patients with severe COVID-19 also contained antibodies against ISG⁺ cells by directly applying serum to peripheral blood mononuclear cells (PBMCs) from healthy individuals, cultured with and without IFN α (Extended Data Fig. 9a–d). We detected the presence of antibodies binding IFN-treated cells in serum from two patients with mild–moderate COVID-19 and two with severe COVID-19 (Extended Data Fig. 9a). However, staining was highly variable for different cell types (Extended Data Fig. 9b–c), both with and without prior IFN α stimulation, suggesting that patients may each have unique combinations of specificities. For instance, although serum from patient 1050 did not stain ISG⁺ cells directly, we found evidence of antibodies against IFN α in this patient (Fig. 3e)—consistent with a recent study¹⁴ that also found anti-IFN α antibodies were present in approximately 12% of patients with COVID-19. This patient was unique in our cohort and IFN α reactivity does not explain the lack of ISG⁺ cells in the majority of patients with severe COVID-19.

We separately tested whether factors in the serum of patients with severe COVID-19 affect the induction of ISG-signature genes in response to IFN α , using IFITM3 as a marker. We thus added patient serum at 5% to a sample of healthy PBMCs stimulated with IFN α and found that, whereas serum from healthy control individuals or from patients with mild–moderate COVID-19 had no effect on differentiation (as measured either by the level of IFITM3 or by the frequency of CD14⁺CD16⁺ intermediate monocytes produced), all tested sera from patients with severe COVID-19 had marked effects, varying from complete block to partial inhibition of the IFN α response (Fig. 3e, g, Extended Data Fig. 9d, e).

To test whether antibodies in the serum of patients with severe COVID-19 were responsible for this inhibition of the IFN α response, we pre-adsorbed patient serum with protein A and protein G (protein A/G) beads to deplete the sera of antibodies. This relieved the block in IFITM3 induction and restored the total yield of interferon-stimulated monocytes (Fig. 3f, g). A similar block and release through antibody absorption was observed for IFN α -dependent generation of the ISG signature in other populations including lymphocytes (Fig. 3h, Extended Data Fig. 9f). It is likely, as robust IFN responses are dependent on a positive feedback loop from initial interferon- α receptor (IFNAR) signalling¹⁵, that the IFN response in lymphocytes benefits from an amplification of IFNAR signalling in monocytes. We also confirmed an inhibition of the generation of ISG⁺ cell populations by serum from patients with severe COVID-19 in a second validation cohort composed of eight patients with mild–moderate COVID-19 and six with severe COVID-19 (Extended Data Fig. 10a, Supplementary Table 2).

Antagonism of IFNAR signalling via FC γ RIIb

Probing the mechanism for this result, we found that treating PBMCs with blocking antibodies to Fc receptors (CD16, CD64 and CD32) during culture with IFN α and patient serum restored the induction of IFITM3 in cells cultured with serum from patients with severe COVID-19 in both

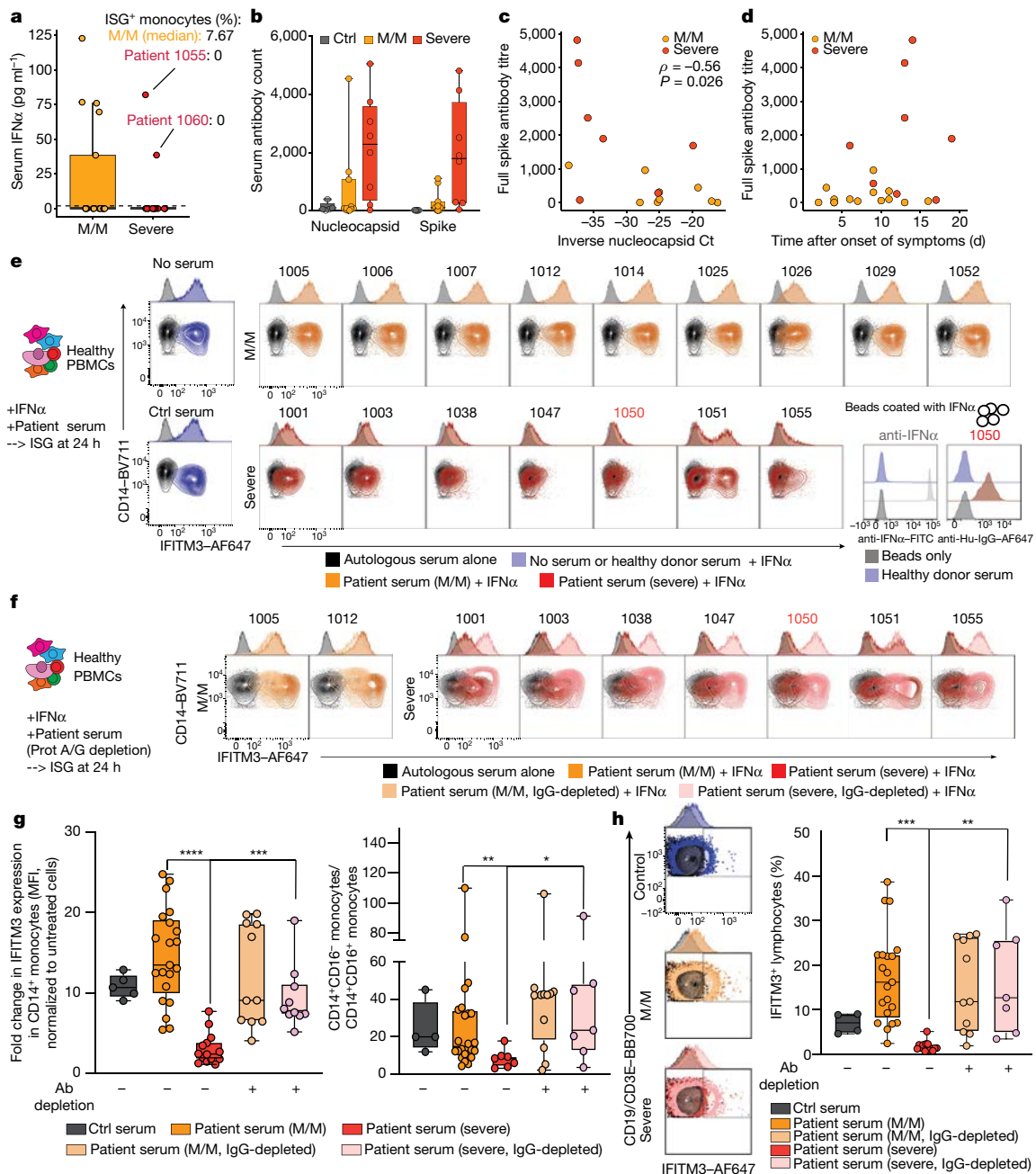


Fig. 3 | Neutralization of ISG induction by antibodies from patients with severe COVID-19. **a**, Serum IFNα concentration in patients with mild–moderate disease ($n = 17$) or severe disease ($n = 15$) who were negative or positive for SARS-CoV-2 (as measured by enzyme-linked immunosorbent assay (ELISA)). Patients 1055 and 1060 are highlighted in red and their frequency of ISG⁺ monocytes (from Fig. 2c) is noted, as is the median frequency for patients with mild–moderate COVID-19. Centre line, median; box limits, 25th and 75th percentiles; whiskers, $1.5 \times$ interquartile range. **b**, Levels of anti-SARS-CoV-2 antibodies (against the spike and nucleocapsid proteins) in serum from patients by Luminex assay. **c**, Scatter plot showing viral load versus levels of antibody binding the SARS-CoV-2 nucleocapsid protein for patients who were positive for SARS-CoV-2, with disease severity overlaid. Antibody levels (full antibody titres against the SARS-CoV-2 spike protein) are shown as arbitrary units of median fluorescence intensity (MFI) from a Luminex assay; viral load is represented by an inverse C_t number from quantitative PCR with reverse transcription (qRT-PCR) with target amplification of the SARS-CoV-2 nucleocapsid sequence. Correlation coefficient and significance were calculated using Spearman's method. Patients for whom data were unavailable were excluded (M/M, $n = 9$; severe, $n = 7$). **d**, Scatter plot showing full antibody titres against the SARS-CoV-2 spike protein relative to days after onset of symptoms. Patients for whom data were unavailable

were excluded (M/M, $n = 14$; severe, $n = 8$). **e**, Contour plots and histograms of CD14 and IFITM3 expression by monocytes after culturing healthy PBMCs with IFNα and serum from healthy donors or from patients with mild–moderate or severe COVID-19. Patient identifiers (1005, 1006 and so on) are shown at the top. **f**, Contour plots and histograms of CD14 and IFITM3 expression by monocytes after pre-treating sera from patients with mild–moderate (light yellow) or severe (pink) COVID-19 with protein A/G beads before incubation with PBMCs, to deplete IgG levels. **g**, Left, Fold change in IFITM3 expression in CD14⁺ monocytes (control, $n = 5$; M/M, $n = 21$; severe, $n = 14$; M/M depleted, $n = 11$; severe depleted, $n = 10$). Right, ratio of classical to intermediate monocytes (control, $n = 4$; M/M, $n = 24$; severe, $n = 7$; M/M depleted, $n = 11$; severe depleted, $n = 7$), from two different experiments and two different healthy donors. **h**, Left, contour plots and histograms of IFITM3 expression by pooled CD3⁺CD19⁺ lymphocytes after culturing healthy PBMCs with IFNα and serum from healthy donors or from patients with mild–moderate or severe disease who were positive for SARS-CoV-2. Right, IFITM3 induction in lymphocytes. Statistical significance in **g**, **h** was assessed using a two-way ANOVA test with multiple comparisons. * $P < 0.05$, ** $P < 0.01$, *** $P < 0.001$, **** $P < 0.0001$. For box plots in **b**, **g**, **h**: centre line, median; box limits, 25th and 75th percentiles; whiskers, minimum and maximum values.

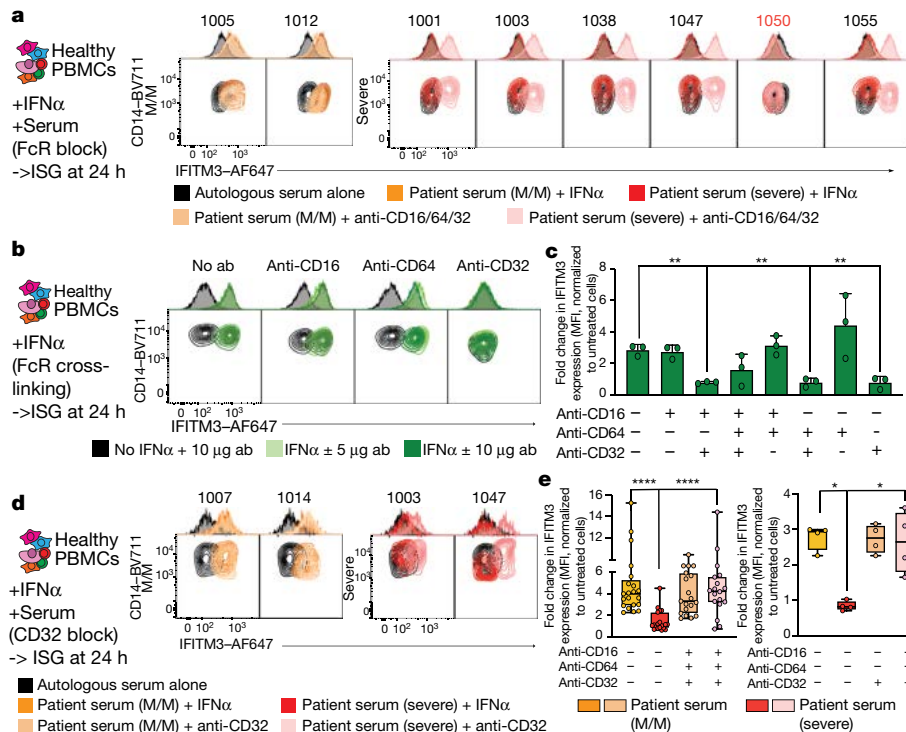


Fig. 4 | IgG-mediated neutralization of ISG induction by serum from patients with severe COVID-19 occurs through binding of the Fc domain of patient antibodies to CD32. a, Contour plots and histograms of CD14 and IFITM3 expression by monocytes after culturing healthy PBMCs with IFN α and serum from healthy donors or from patients with mild–moderate or severe COVID-19, in the presence or absence of anti-CD16, anti-CD64 and anti-CD32 antibodies (anti-CD16/64/32) to block Fc receptors (FcRs). Patient identifiers are shown at the top. **b**, **c**, Contour plots and histograms of CD14 and IFITM3 expression (**b**) and fold change in IFITM3 expression (**c**) in CD14⁺ monocytes after culturing healthy PBMCs with or without IFN α and with or without 5 or 10 μ g ml⁻¹ of plate-coated isotype control, anti-CD16, anti-CD32 or anti-CD64

discovery (Fig. 4a, e) and validation (Extended Data Fig. 10b) cohorts. Blocking Fc receptors restored not only the induction of IFITM3, but also that of other ISGs, such as IFI27, ISG15 and MX1 (Extended Data Fig. 10c). These results, together with the absence of an increase in cell deaths in PBMCs cultured with serum from patients with severe COVID-19 (Extended Data Fig. 10d), suggested that antibodies that are present in the serum of patients with severe disease trigger Fc receptor signalling, which inhibits transcriptional responses after IFNAR engagement.

We considered that such a mechanism might represent a fundamental way for antibody generation to downregulate an interferon cascade, and therefore we tested whether activating Fc receptors via cross-linking antagonized the induction of IFITM3 induction by IFN α . PBMCs that were subjected to individual cross-linking of CD32 exhibited markedly less induction of IFITM3 than PBMCs subjected to individual cross-linking of CD16 and CD64 (Fig. 4b, c, Extended Data Fig. 10e), whereas cross-linking of all three Fc receptors together induced the production of pro-inflammatory cytokines (Extended Data Fig. 10f).

Returning to the effects of serum from patients with severe COVID-19, we found that blocking CD32 alone restored the induction of IFITM3 in PBMCs cultured with IFN α in the presence of serum from patients with severe COVID-19 (Fig. 4d, e). Previous studies have shown that blockade of Fc γ receptor IIb (Fc γ RIIb; also known as CD32B) blockade leads to interferon-like responses in dendritic cells and monocytes¹⁶, whereas binding of the activating Fc receptor Fc γ RIIa (CD32A) elicits viral immunity¹⁷. Consistent with these previous studies, we found that blockade of Fc γ RIIb, but not that of Fc γ RIIa, rescued the induction of

antibodies alone or in combination to cross-link and activate Fc receptors. Results in **c** are from two independent experiments and two different cell donors, including two antibody quantities for one of the donors ($n = 3$ experiments). Data are mean \pm s.d. **d**, Neutralization assay as presented in **a**, but with the sole addition of anti-CD32 antibodies. **e**, Fold changes in IFITM3 expression for experiments in **a** (left) (five independent experiments and three different donors) and **d** (right) (one experiment and two different donors). Centre line, median; box limits, 25th and 75th percentiles; whiskers, minimum and maximum values. Statistical significance in **c**, **e** was assessed using a two-way ANOVA with multiple comparisons. * $P < 0.05$, ** $P < 0.01$, **** $P < 0.0001$.

IFITM3 in monocytes cultured with serum from patients with severe COVID-19 (Extended Data Fig. 10g).

Together, our findings suggest that inhibition of a phenotype of ISG-expressing populations of immune cells in patients with severe COVID-19 corresponds to antagonism of IFNAR signalling via Fc γ RIIb signalling by their antibodies. In our cohort, this general antibody-mediated effect manifests in almost all patients with severe disease, whereas antibodies against the cytokine IFN α itself were seen in only one of seven patients, and those antibodies blocked ISG function but not through Fc receptors (Fig. 4a). With regard to specificity, it is notable that recent studies have highlighted that auto-antibodies in patients with COVID-19 bind to targets as diverse as phospholipids¹⁸ and endothelial proteins¹⁹, but that not all patients had developed each specificity. Our work has likewise found that antibodies bind to a variety of immune cells and it is possible that, in the course of some infections, incomplete tolerance in the B cell compartment may include recognition of a great many host proteins, including those on immune cells. Although it will be important to study the probable diverse nature of antibody specificities in COVID-19, afucosylation of antibodies—which modifies the selectivity of antibodies for Fc receptor subtypes—and differential IgG subclass selectivity are also emerging as distinguishing features of COVID-19 severity²⁰. We speculate that variable levels of these IgG subclasses in sera, combined with varying affinities for different Fc receptors, could result in stronger signalling through inhibitory Fc γ RIIb. Further work will be necessary to characterize the relative contributions of these IgG subclasses and their specificities. Regardless, our study suggests that this global targeting of ISG archetypes in

patients with severe COVID-19 might be addressable with drugs such as rituximab to reduce B cell responses²¹—perhaps in the presence of serum from convalescent individuals, through the introduction of intravenous IgG (IVIG) to compete with serum antibodies for Fc receptor engagement²², or with rapid development of antibodies that clinically block FCγRIIb.

Online content

Any methods, additional references, Nature Research reporting summaries, source data, extended data, supplementary information, acknowledgements, peer review information; details of author contributions and competing interests; and statements of data and code availability are available at <https://doi.org/10.1038/s41586-021-03234-7>.

- Mathew, D. et al. Deep immune profiling of COVID-19 patients reveals distinct immunotypes with therapeutic implications. *Science* **369**, eabc8511 (2020).
- Schulte-Schrepping, J. et al. Severe COVID-19 is marked by a dysregulated myeloid cell compartment. *Cell* **182**, 1419–1440 (2020).
- Hadjadj, J. et al. Impaired type I interferon activity and inflammatory responses in severe COVID-19 patients. *Science* **369**, 718–724 (2020).
- Zilionis, R. et al. Single-cell transcriptomics of human and mouse lung cancers reveals conserved myeloid populations across individuals and species. *Immunity* **50**, 1317–1334 (2019).
- Huang, I. C. et al. Distinct patterns of IFITM-mediated restriction of filoviruses, SARS coronavirus, and influenza A virus. *PLoS Pathog.* **7**, e1001258 (2011).
- Reyes, M. et al. An immune-cell signature of bacterial sepsis. *Nat. Med.* **26**, 333–340 (2020).
- Davizon-Castillo, P., Rowley, J. W. & Rondina, M. T. Megakaryocyte and platelet transcriptomics for discoveries in human health and disease. *Arterioscler. Thromb. Vasc. Biol.* **40**, 1432–1440 (2020).
- Mason, K. D. et al. Programmed anuclear cell death delimits platelet life span. *Cell* **128**, 1173–1186 (2007).
- Bongiovanni, D. et al. Transcriptome analysis of reticulated platelets reveals a prothrombotic profile. *Thromb. Haemost.* **119**, 1795–1806 (2019).
- Chen, W. S. et al. Uncovering axes of variation among single-cell cancer specimens. *Nat. Methods* **17**, 302–310 (2020).
- Pujadas, E. et al. SARS-CoV-2 viral load predicts COVID-19 mortality. *Lancet Respir. Med.* **8**, e70 (2020).

- Hue, S. et al. Uncontrolled innate and impaired adaptive immune responses in patients with COVID-19 ARDS. *Am. J. Respir. Crit. Care Med.* **202**, 1509–1519 (2020).
- Wang, Y. et al. Kinetics of viral load and antibody response in relation to COVID-19 severity. *J. Clin. Invest.* **130**, 5235–5244 (2020).
- Bastard, P. et al. Autoantibodies against type I IFNs in patients with life-threatening COVID-19. *Science* **370**, eabd4585 (2020).
- Michalska, A., Blaszczyk, K., Wesoly, J. & Bluyssen, H. A. R. A positive feedback amplifier circuit that regulates interferon (IFN)-stimulated gene expression and controls type I and type II IFN responses. *Front. Immunol.* **9**, 1135 (2018).
- Dhodapkar, K. M. et al. Selective blockade of the inhibitory Fcγ receptor (FcγRIIb) in human dendritic cells and monocytes induces a type I interferon response program. *J. Exp. Med.* **204**, 1359–1369 (2007).
- Bournazos, S., Corti, D., Virgin, H. W. & Ravetch, J. V. Fc-optimized antibodies elicit CD8 immunity to viral respiratory infection. *Nature* **588**, 485–490 (2020).
- Zuo, Y. et al. Prothrombotic autoantibodies in serum from patients hospitalized with COVID-19. *Sci. Transl. Med.* **12**, eabd3876 (2020).
- Consiglio, C. R. et al., The immunology of multisystem inflammatory syndrome in children with COVID-19. *Cell* **183**, 968–981 (2020).
- Chakraborty, S. et al. Proinflammatory IgG Fc structures in patients with severe COVID-19. *Nat. Immunol.* **22**, 67–73 (2021).
- Huang, H., Benoist, C. & Mathis, D. Rituximab specifically depletes short-lived autoreactive plasma cells in a mouse model of inflammatory arthritis. *Proc. Natl Acad. Sci. USA* **107**, 4658–4663 (2010).
- John Looney, R. & Huggins, J. Use of intravenous immunoglobulin G (IVIG). *Best Pract. Res. Clin. Haematol.* **19**, 3–25 (2006).

Publisher's note Springer Nature remains neutral with regard to jurisdictional claims in published maps and institutional affiliations.

© The Author(s), under exclusive licence to Springer Nature Limited 2021

The UCSF COMET Consortium

Cai Cathy^{1,2}, Jenny Zhan^{1,2}, Bushra Samad^{1,2}, Suzanna Chak⁵, Rajani Ghale⁵, Jeremy Giberson^{5,15}, Ana Gonzalez^{5,15}, Alejandra Jauregui⁵, Deanna Lee^{5,6,15}, Viet Nguyen^{5,6,15}, Kimberly Yee^{5,6}, Yumiko Abe-Jones¹⁴, Logan Pierce¹⁴, Priya Prasad¹⁴, Pratik Sinha⁵, Alexander Beagle⁵, Tasha Lea¹, Armond Esmalji¹⁴, Austin Sigman⁵, Gabriel M. Ortiz¹⁵, Kattie Raffel¹⁴, Chayse Jones⁵, Kathleen Liu^{5,17} & Walter Eckalbar^{3,5}

¹⁵Zuckerberg San Francisco General Hospital and Trauma Center, University of California San Francisco, San Francisco, California, USA. ¹⁶Division of Nephrology, Department of Medicine, University of California San Francisco, San Francisco, California, USA. ¹⁷Division of Critical Care Medicine, Department of Anesthesia, University of California at San Francisco, San Francisco, CA, USA.

Methods

Data reporting

No statistical methods were used to predetermine sample size. The experiments were not randomized and the investigators were not blinded to allocation during experiments and outcome assessment.

Patients, participants, severity score and clinical data collection

Patients admitted to the Hospital of the University of California with known or presumptive COVID-19 were screened within three days of hospitalization. Patients, or a designated surrogate, provided informed consent to participate in the study. This study includes a subset of patients enrolled between 8 April and 1 May 2020 in the COMET (COVID-19 Multi-immunophenotyping projects for Effective Therapies; <https://www.comet-study.org/>) study at the University of California San Francisco (UCSF). COMET is a prospective study that aims to describe the relationship between specific immunological assessments and the clinical courses of COVID-19 in hospitalized patients. Healthy donors (control individuals) were adults with no prior diagnosis of or recent symptoms consistent with COVID-19. This analysis includes samples from participants who provided informed consent directly, via a surrogate, or otherwise in accordance with protocols approved by the regional ethical research boards and the Declaration of Helsinki. For in-patients, clinical data were abstracted from the electronic medical record into standardized case report forms. We used a severity score both at the time of sampling and at the end of hospitalization (Extended Data Fig. 1a). In both cases, severity assessment was based on three main parameters: level of care, need for mechanical ventilation and time under mechanical ventilation. Patients classified as having mild–moderate disease are patients who were on a standard hospital ward or in the intensive care unit (ICU) who did not require mechanical ventilation during their time of hospitalization and spent no more than one day in ICU. Patients classified as having mild–moderate disease are patients who required intensive care and mechanical ventilation (typically five days or more). Therefore, our validation cohort is composed of 21 patients with COVID-19 (11 mild–moderate and 10 severe); 11 patients with a similar clinical presentation but who did not have COVID-19 (6 mild–moderate and 5 severe); and 14 healthy control individuals. We also collected and used serum from a validation cohort composed of 14 patients who were positive for SARS-CoV-2. Samples were collected and severity was assessed as previously described for the initial cohort. This discovery cohort is composed of 8 patients with mild–moderate COVID-19 and 6 patients with severe COVID-19. Information on age, sex, type of infection, day of onset, viral load and complete blood cell count is listed in Supplementary Table 1. The study is approved by the UCSF Institutional Review Board: IRB 20-30497.

Isolation of blood cells and processing for scRNA-seq

scRNA-seq was performed on fresh whole blood to preserve granulocytes. In brief, peripheral blood was collected into EDTA tubes (BD, 366643). Whole blood was prepared by treatment of 500 μ l of peripheral blood with RBC lysis buffer (Roche, 11-814-389-001) according to the manufacturer's instructions. Cells were then counted and 15,000 cells per individual were directly loaded in the Chromium Controller for partitioning single cells into nanolitre-scale gel bead-in-emulsions (GEMs) following the manufacturer's instructions (10X Genomics). Some samples were pooled together (at 15,000 cells per sample) before GEM partitioning. A Chromium Single Cell 5' Reagent Kit (v.5.1) (10X Genomics) was used for reverse transcription, cDNA amplification and library construction of the gene expression libraries (following the detailed protocol provided by 10X Genomics). Libraries were sequenced on an Illumina NovaSeq6000 using 28 cycles for R1 and 98 cycles for R2. All samples were encapsulated, and cDNA was generated within 6 h after blood draw.

PBMC co-culture experiment with patient serum and flow cytometry analysis

PBMCs were isolated from EDTA-anticoagulated whole blood from healthy donors using PolymorphPrep (Alere Technologies), and resuspended in culture medium (RPMI 1640 + 10% FBS). For detection of neutralization of interferon stimulation, autologous serum or serum from clinical study participants (10 μ l) was plated with IFN α (Stemcell IFN α -2A; final concentration of 1 μ g μ l⁻¹) in a total volume of 200 μ l before addition of 2.5×10^5 PBMCs. After incubation for 24 h, PBMCs were assayed for IFN α -induced IFITM3 upregulation and CD14 and CD16 levels and fractions by flow cytometry. After surface staining and addition of fixable live/dead violet dye (Thermo Fisher Scientific, L34955), intracellular detection of IFITM3 was done using the eBioscience Foxp3/Transcription Factor Staining Buffer Set (Thermo Fisher Scientific, 00-5523-00), following the manufacturer's instructions. For Fc receptor blocking experiments, Fc receptors were blocked with unconjugated anti-CD16 (clone 3G8; BioLegend, 302002), anti-CD32 (clone FUN-2; BioLegend, 303202), anti-CD64 (clone 10.1; BioLegend, 305002), anti-CD32A (clone IV.4; BioXcell) and anti-CD32B/C (clone SI8005H; BioLegend) with 0.5 μ g of each antibody. After incubation for 24 h with IFN α (1 μ g μ l⁻¹), PBMCs were assayed for IFN α -induced IFITM3 upregulation and CD14 and CD16 levels and fractions by flow cytometry. For serum staining assays, PBMCs were cultured with medium or 1–100 μ g ml⁻¹ IFN α for 38–46 h. Samples were collected and Fc receptors were blocked with unconjugated anti-CD16 (clone 3G8; BioLegend, 302002), anti-CD32 (clone FUN-2; BioLegend, 303202) and anti-CD64 (clone 10.1; BioLegend, 305002) antibodies for 20 min on ice. After one washing step with fluorescence-activated cell sorting (FACS) buffer (2% fetal bovine serum, 1 mM EDTA, PBS), non-specific binding of the detection antibody was blocked by incubating with unconjugated AffiniPure donkey anti-human IgG (Jackson ImmunoResearch; 709-005-149) for 15 min at room temperature. After washing with FACS buffer, PBMCs were then stained for surface markers for 30 min on ice. After staining incubation, cells were washed 3 times with FACS buffer (1,500 rpm, 5 min, 4 °C) and incubated with 5 μ l autologous serum or serum from clinical study participants for 30 min on ice. After washing the cells with FACS buffer, cell-bound antibodies were detected using an AffiniPure donkey anti-human IgG–Alexa Fluor 647 antibody (Jackson ImmunoResearch, 709-605-149), which was incubated with the cells for 30 min on ice. Cells were washed again and resuspended in 1 μ g ml⁻¹ DAPI solution for live/dead discrimination. The following antibodies were used for flow cytometric analysis: anti-human CD3–BB700 (clone SK7; BD Biosciences, 566575), anti-human CD14–BV711 (clone MSE2; BioLegend, 301838), anti-human CD15–BV786 (clone W6D3; BD Biosciences, 741013), anti-human CD16–BV605 (clone 3G8; BioLegend, 302040), anti-human CD19–BV785 (clone HIB19; BioLegend, 302240), anti-human CD45–APCeFluor780 (clone HI30; Thermo Fisher Scientific, 47-0459-42), anti-human IFITM3–AlexaFluor 647 (clone EPR5242; Abcam, ab198573).

Fc-receptor cross-linking experiment in PBMCs

Flat-bottom polystyrene plates (96-well) were coated overnight at 4 °C with either 10 or 5 μ g ml⁻¹ of combinations of anti-CD16 (clone 3G8; BioLegend, 302002), anti-CD32 (clone FUN-2; BioLegend, 303202) and anti-CD64 (clone 10.1; BioLegend, 305002) diluted in PBS. Plates were washed three times with PBS before PBMC plating, which was prepared as detailed above. A total of 250,000 PBMCs per well were spun down briefly and incubated at 37 °C for 15 min to allow for coated antibody engagement. IFN α was then added into the well and cells were incubated for 24 h at 37 °C before flow cytometry as described above.

Statistical analysis and data visualization

Statistical analyses were performed using GraphPad Prism or the R software package. Null hypotheses between two groups were tested

Article

using the nonparametric Mann–Whitney test to account for non-normal distribution of the data. Likewise, for multiple groups, comparisons were made by two-way ANOVA or nonparametric Kruskal–Wallis test followed by multiple comparisons. The specific statistical tests and their resulting significance levels are also noted in each figure legend. The R packages Seurat and ggplot2 (v.3.1.0), GraphPad Prism and Adobe Illustrator were used to generate figures.

Reporting summary

Further information on research design is available in the Nature Research Reporting Summary linked to this paper.

Data availability

The data reported are in the Article and its associated Supplementary Informations. Cell-Ranger-processed raw feature–barcode matrices are available at the Gene Expression Omnibus (GEO) with accession number GSE163668, and raw FASTQ files for all 10X libraries have been deposited in the Sequence Read Archive (SRA) with accession number SRP299788.

Code availability

Scripts used to process all data, along with relevant clinical information for each patient, are available at https://github.com/UCSF-DSCOLAB/combes_et_al_COVID_2020.

23. Villani, A.-C. et al. Single-cell RNA-seq reveals new types of human blood dendritic cells, monocytes, and progenitors. *Science* **356**, eaah4573 (2017).
24. Argüello, R. J. et al. SCENITH: a flow cytometry-based method to functionally profile energy metabolism with single-cell resolution. *Cell Metab.* **32**, 1063–1075 (2020).

Acknowledgements We thank all members of the Krummel laboratory and ImmunoX for discussion and guidance while developing this study, and we thank G. Andreoletti for discussion and guidance on computational analysis. This work was supported by funds from the UCSF ImmunoX Initiative and funds from the NIH (R01 AI52116-S1 (M.F.K.) 3U19AI077439-13S1 (D.J.E.) and NHLBI R35 HL140026 (C.C.)). K.H.H. is supported by the American Cancer Society Postdoctoral Fellowship (133078-PF-19-222-01-LIB). A.R. is a Cancer Research Institute Irvington Postdoctoral Fellow supported by the Cancer Research Institute (award number CRI2940). This project has been made possible in part by grant number 2019-202665 from the Chan Zuckerberg Foundation.

Author contributions A.J.C., T.C., N.F.K., K.H.H., A.R., A.A.R., W.S.C., N.W.C., S.J.C. and M.F.K. performed and provided supervision of experiments, generated and analysed data and contributed to the manuscript by providing figures and tables. A.J.C., T.C., N.F.K., K.H.H., A.R., A.A.R. and M.F.K. had full access to all of the data in the study and take responsibility for the integrity of the data and the accuracy of the analyses. A.J.C., T.C., N.F.K., K.H.H., A.R., A.A.R. and W.S.C. performed computational analyses of the data. A.J.C., T.C., K.H.H., V.C., N.W.C., D.K., G.C.R., A.S., J.T., K.J.H.-G., P.M.-S., W.S.Z., D.S.L. and Y.S. were part of the early-morning COVID-19 processing team who performed the whole-blood single-cell sequencing. The UCSF COMET Consortium included all other scientists involved in the generation of data included in this study. C.L. provided data on viral loads obtained from nasal swabs of patients with COVID-19. C.J.Y., M.R.L. and S.J.C. provided blood from healthy donors and helped with PBMC preparation. N.K.S., K.W.I., R.Y., M. Magnen, L.R., A.L., C.R.Z. and R.P.L. performed assays of SARS-CoV-2 infection and serum antibodies and cytokines. M.R.W. and M. Matthey oversaw studies of serum cytokines and antibodies from the COVID-19 patient cohort and provided intellectual input. P.G.W., D.J.E., G.K.F., C.C., C.L., C.H., K.K. and M.F.K. are leadership members of the COMET study and were actively involved in the establishment of the pipeline and patient consent and the direction of projects. P.G.W., C.C., C.M.H., A.W. and S.C. actively participated in the enrolment of patient and control cohorts. A.J.C., T.C., N.F.K., K.H.H., A.R., A.A.R., W.S.C. and M.F.K. wrote the manuscript. A.J.C., A.A.R. and M.F.K. supervised the project. All authors edited and critically revised the manuscript for important intellectual content and gave final approval for the version to be published.

Competing interests The authors declare no competing interests.

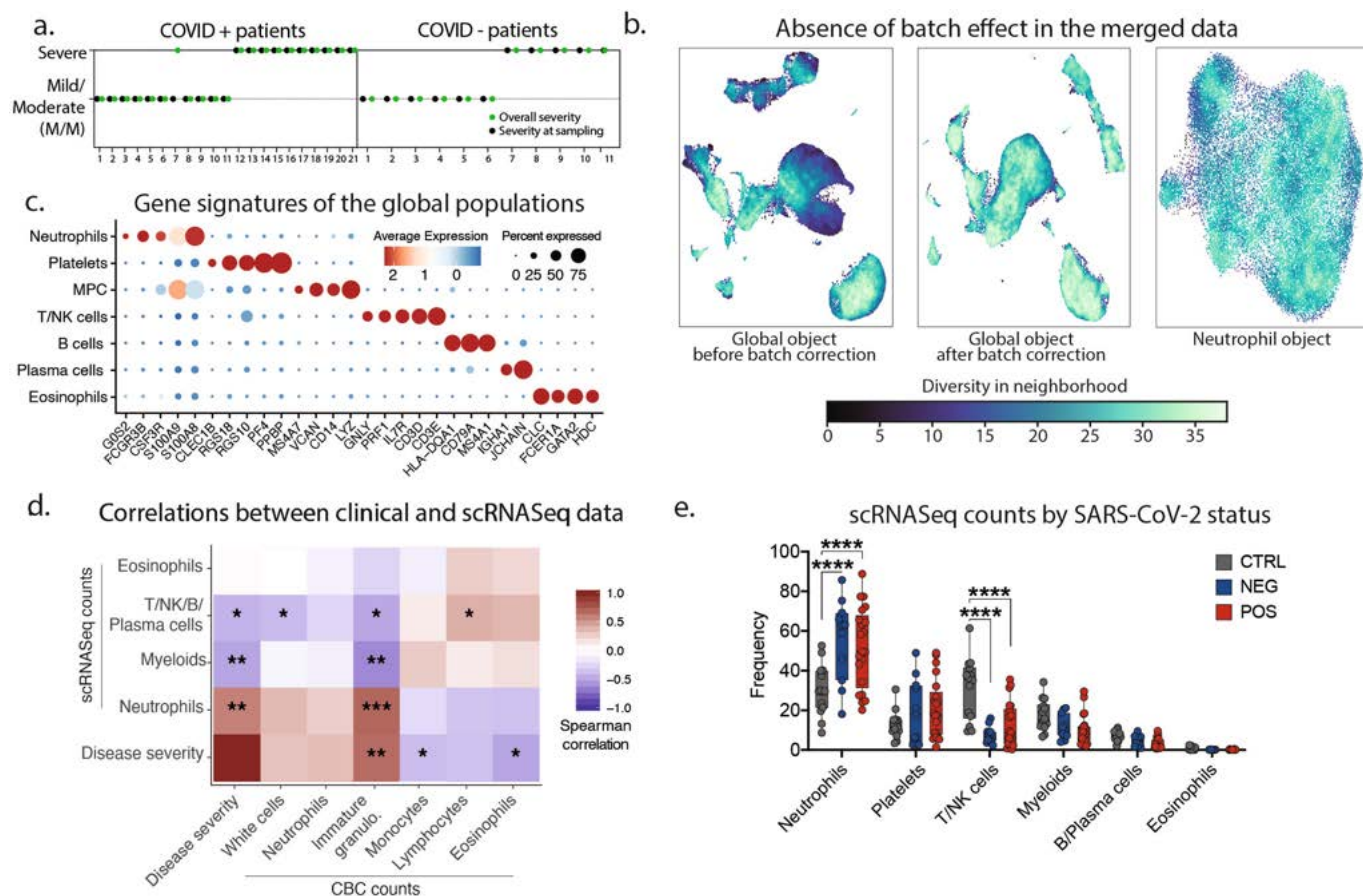
Additional information

Supplementary information The online version contains supplementary material available at <https://doi.org/10.1038/s41586-021-03234-7>.

Correspondence and requests for materials should be addressed to A.J.C., A.A.R. or M.F.K.

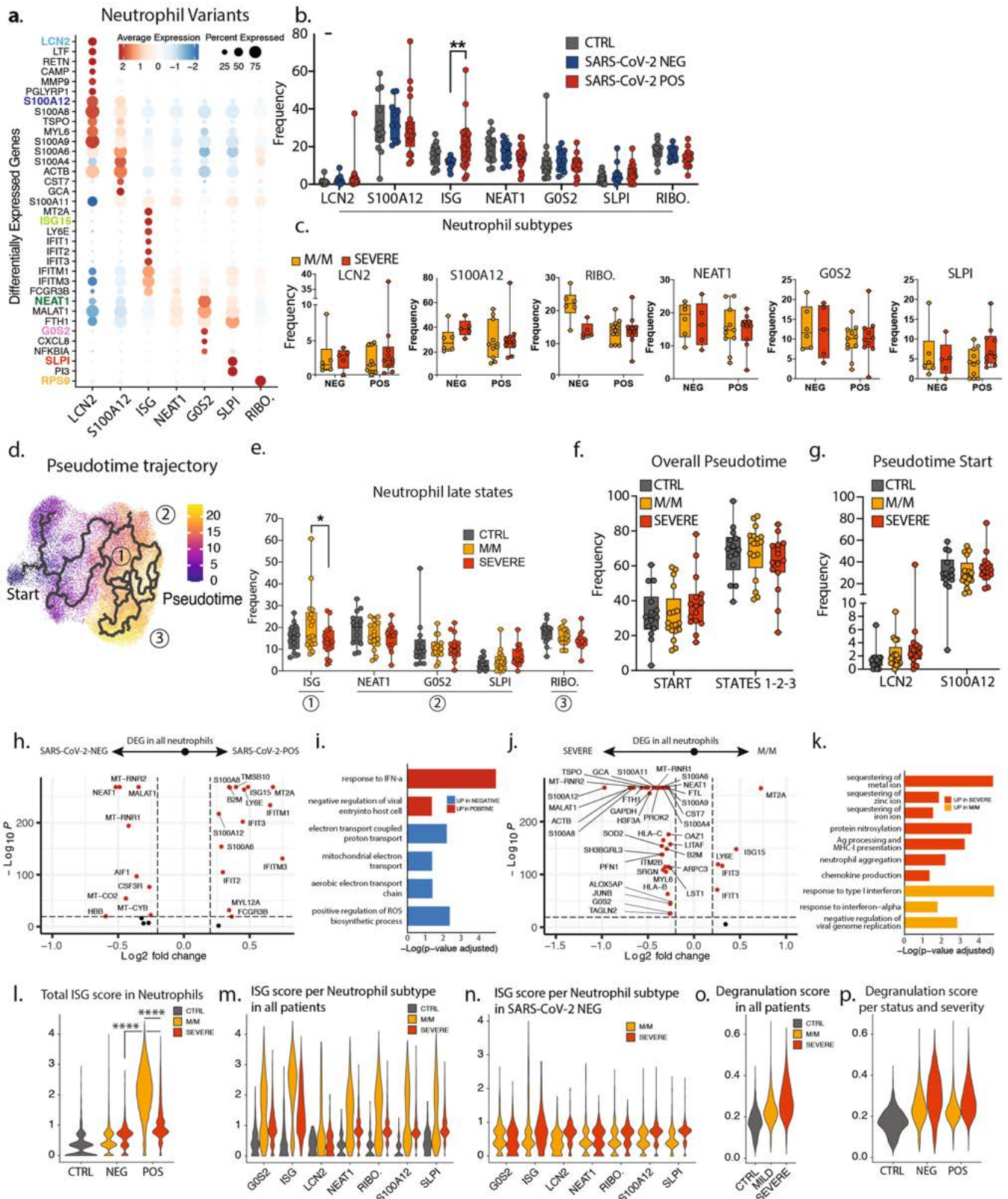
Peer review information Nature thanks Petter Brodin, Eric Meffre and the other, anonymous, reviewer(s) for their contribution to the peer review of this work. Peer reviewer reports are available.

Reprints and permissions information is available at <http://www.nature.com/reprints>.



Extended Data Fig. 1 | Immune phenotyping of patients admitted with respiratory symptoms using whole-blood scRNA-seq. a, Patient symptoms plot: symptoms at day of sampling (first day of admission to the hospital) are in black; symptoms on the basis of the entire course of hospitalization are in green. In the rest of the Article, we categorized patients into mild-moderate or severe cases on the basis of the entire course of hospitalization (green). **b,** Quantification of the batch effect using neighbour diversity score in the global object UMAP before (left) and after (middle) batch correction, along with the neutrophil UMAP plot (right), as in Fig. 1b, c, using the diversity in

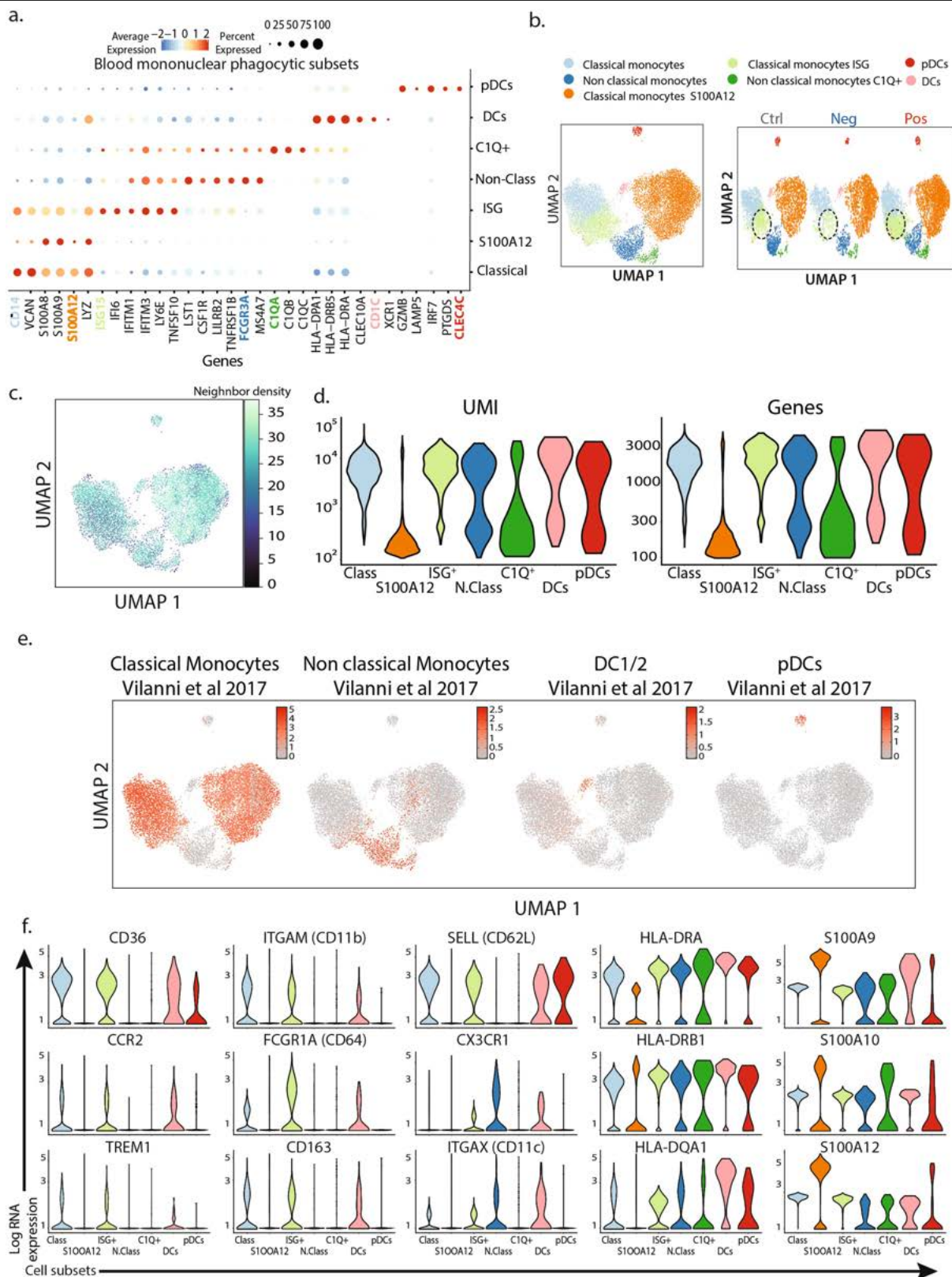
neighbourhood method. **c,** Dot plot representation of landmark genes expressed by global populations in Fig. 1b. MPC, mononuclear phagocyte cells. **d,** Spearman's correlation comparison between disease severity and population frequencies calculated from 10X scRNA-seq analyses (10X) or complete blood cell counts. Patients for whom complete blood cell counts were unavailable were excluded. Significance was calculated using Spearman's method. * $P < 0.05$, ** $P < 0.01$, *** $P < 0.001$ ($n = 29$). **e,** Frequency of the global populations in Fig. 1b among all cells by SARS-CoV-2 status (control, $n = 14$; SARS-CoV-negative, $n = 11$; SARS-CoV-positive, $n = 21$).



Extended Data Fig. 2 | See next page for caption.

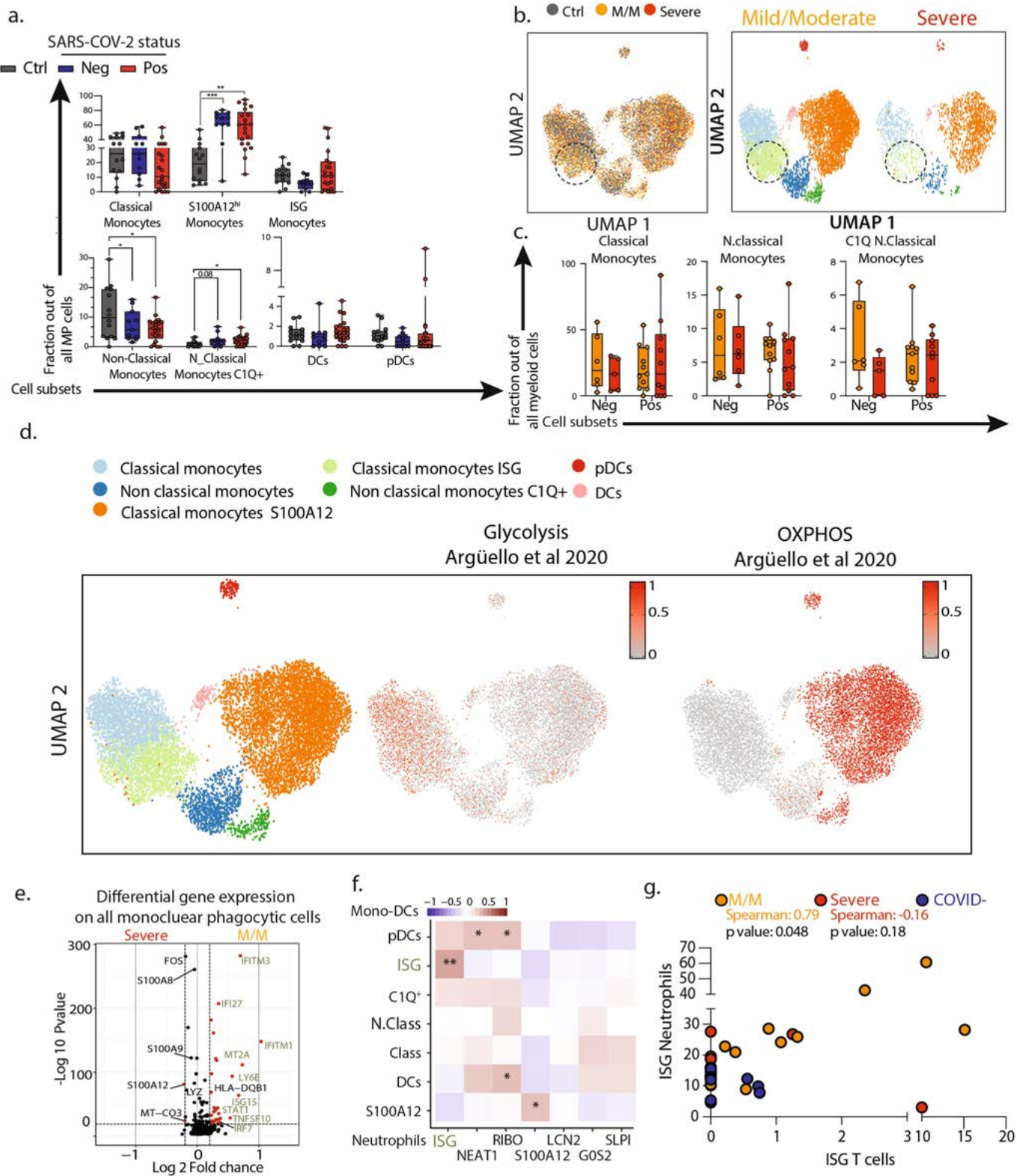
Extended Data Fig. 2 | Patients with severe COVID-19 lack an interferon response in neutrophils. **a**, Dot plot of top DEGs between neutrophil subsets. **b**, Frequencies of neutrophil subsets among all neutrophils across healthy control individuals ($n = 14$), patients who were negative for SARS-CoV-2 ($n = 11$) and patients who were positive for SARS-CoV-2 ($n = 21$). **c**, Frequency of the LCN2, S100A12, RIBO., NEAT1, GOS2 and SLPI neutrophils among all neutrophils, by SARS-CoV-2 status and disease severity (SARS-CoV-2-negative M/M, $n = 6$; SARS-CoV-2-negative severe, $n = 5$; SARS-CoV-2-positive M/M, $n = 11$, SARS-CoV-2-positive severe, $n = 10$). **d**, Pseudotime trajectory of neutrophil subsets. **e**, Frequencies of the neutrophil subsets among all neutrophils at later stages of pseudotime trajectories among healthy control individuals ($n = 14$), patients with mild-moderate disease ($n = 17$) and patients with severe disease ($n = 15$). **f, g**, Frequencies of the neutrophil subsets in all neutrophils across healthy control individuals ($n = 14$), patients with mild-moderate disease ($n = 17$) and patients with severe disease ($n = 15$) at the overall start or late states

of the trajectories (**f**) or at specific early stages of the pseudotime (**g**). **h-k**, Volcano plots showing DEGs (**h, j**) and bar plots showing gene ontology (GO) term enrichment from these DEGs (**i, k**) among all neutrophils from either patients who were positive for SARS-CoV-2 versus those who were negative for SARS-CoV-2 (**h, i**), or patients with mild-moderate disease versus those with severe disease (**j, k**). **l-p**, ISG-signature scores (**l-n**) and neutrophil degranulation (**o, p**) in all neutrophils among healthy control individuals, patients with mild-moderate disease and patients with severe disease (**o**); in all neutrophils according to SARS-CoV-2 status and disease severity (**l, p**); or in specific neutrophil subtypes across severity in either all patients (**m**) or only patients who were negative for SARS-CoV-2 (**n**). Statistical significance was assessed using a two-way ANOVA with multiple comparisons (**c, e, g**) or a two-tailed Wilcoxon test (**l**). * $P < 0.05$, ** $P < 0.01$, *** $P < 0.001$, **** $P < 0.0001$. For box plots: centre line, median; box limits, 25th and 75th percentiles; whiskers, minimum and maximum values.



Extended Data Fig. 3 | Characterization of subsets of peripheral blood mononuclear phagocytes in our cohort. **a**, Dot plot representation of the top DEGs between clusters identified in subsets of blood mononuclear phagocytes. **b**, UMAP visualization of the 19,289 mononuclear phagocytes isolated from the entire dataset (left) and split by SARS-CoV-2 status (right). **c**, Quantification of the batch effect before and after batch correction using neighbour diversity score in the mononuclear phagocytes object from the UMAP plot in **b**, using the diversity in neighbourhood method. **d**, Violin plots of

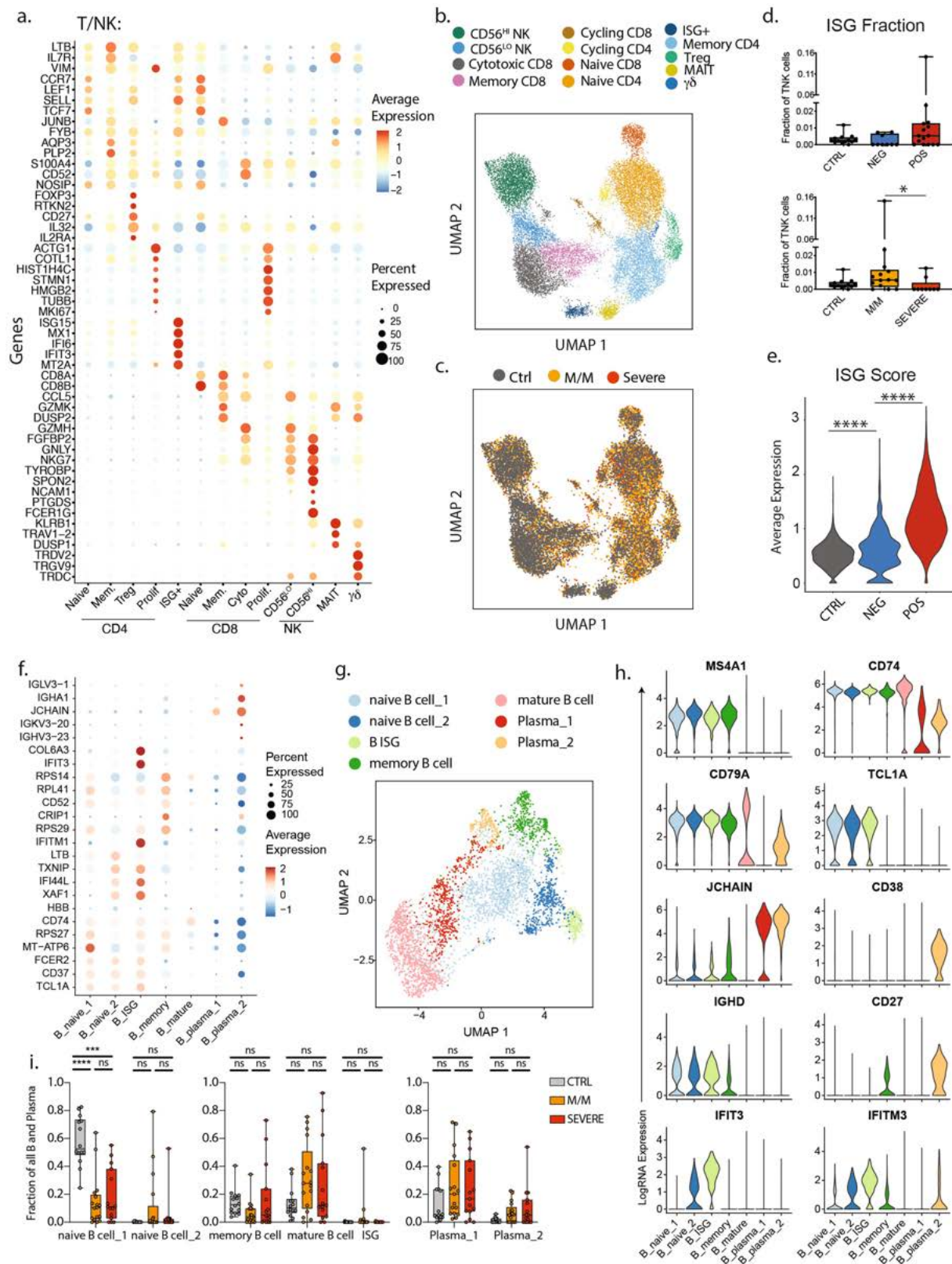
number of unique genes (bottom) and number of unique molecules (top) detected from single-cell sequencing for each cluster identified in the mononuclear phagocytes dataset. **e**, Overlay of previously described blood mononuclear phagocytic cell signatures from a healthy individual²³ on mononuclear phagocytes from the UMAP plot in **b**. **f**, Violin plots of canonical genes that were previously found to be expressed by blood mononuclear phagocytes for each cluster identified in the mononuclear phagocytes dataset.



Extended Data Fig. 4 | See next page for caption.

Extended Data Fig. 4 | Severe COVID-19 is defined by the lack of a concerted interferon response across multiple cell types. **a**, Frequencies of the mononuclear phagocyte subsets among all mononuclear phagocytes in healthy control individuals ($n = 14$), patients who were negative for SARS-CoV-2 ($n = 11$) and patients who were positive for SARS-CoV-2 ($n = 21$). **b**, UMAP visualization of the 19,289 mononuclear phagocytes coloured (left) and split by (right) disease severity. **c**, Frequencies of the classical monocytes, cycling monocytes, nonclassical monocytes and CIQ⁺ nonclassical monocytes among all mononuclear phagocytes in patients who were negative for SARS-CoV-2 (M/M, $n = 6$; severe, $n = 5$) and patients who were positive for SARS-CoV-2 (M/M, $n = 11$; severe, $n = 10$), split by disease severity. **d**, Overlay of previously described²⁴ glycolytic and oxidative phosphorylation gene signatures on mononuclear phagocytes from the UMAP plot in Extended Data Fig. 3b.

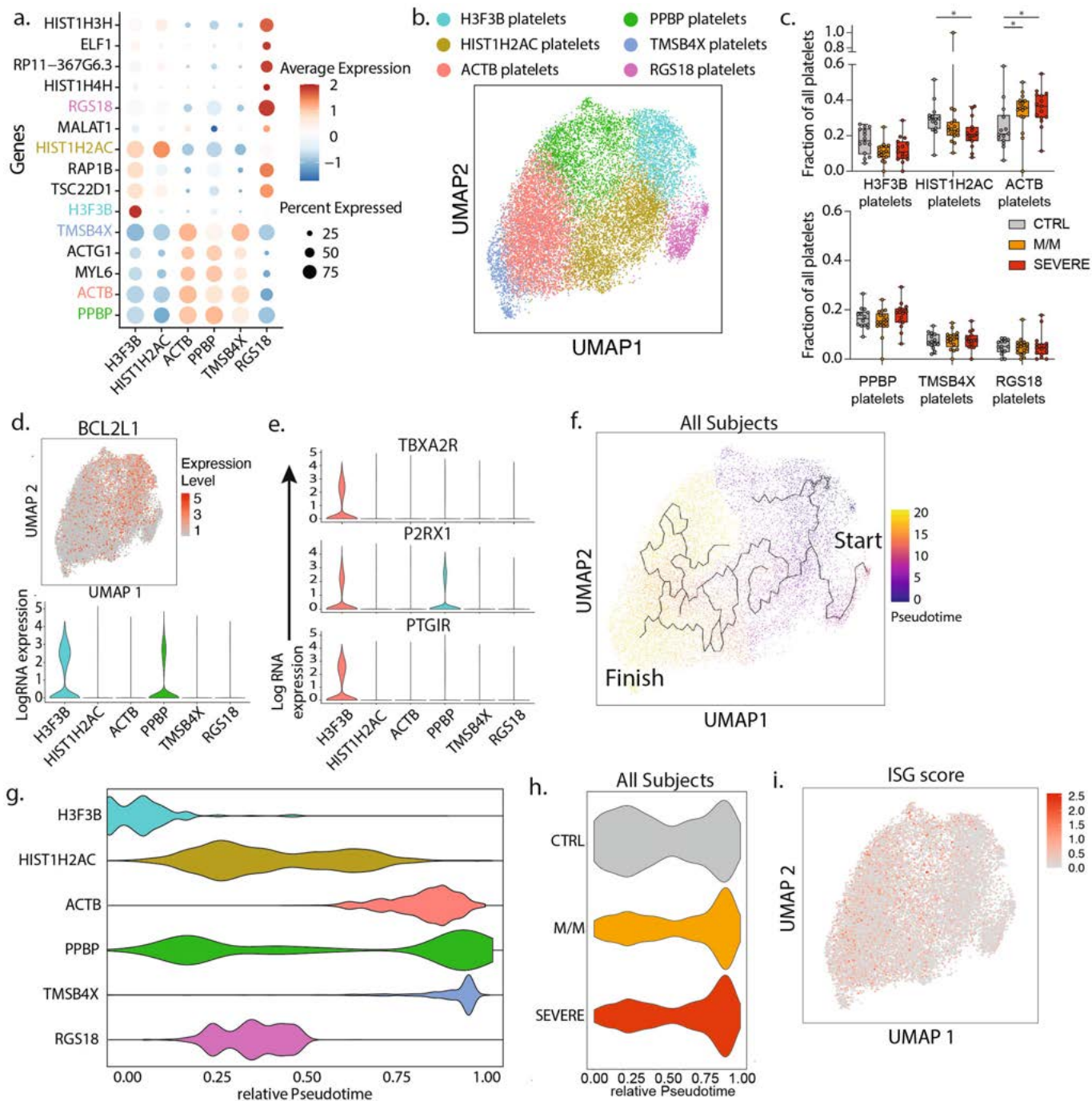
e, Volcano plot showing results of differential gene expression analysis performed on all mononuclear phagocytes among patients with mild-moderate disease (right) and severe disease (left). **f**, Correlation matrix using Spearman rank correlation between the frequency of all neutrophil and monocyte subtypes in all patients who were negative for SARS-CoV-2 ($n = 11$) and all patients who were positive for SARS-CoV-2 ($n = 21$). **g**, Scatter plot between neutrophil and CD4⁺ T cell ISG⁺ subsets in the indicated groups of patients (M/M, $n = 11$; severe, $n = 10$; SARS-CoV-2-negative, $n = 11$). Statistical significance was assessed using a two-way ANOVA with multiple comparisons. * $P < 0.05$, ** $P < 0.01$, *** $P < 0.001$, **** $P < 0.0001$. For box plots: centre line, median; box limits, 25th and 75th percentiles; whiskers, minimum and maximum values.



Extended Data Fig. 5 | See next page for caption.

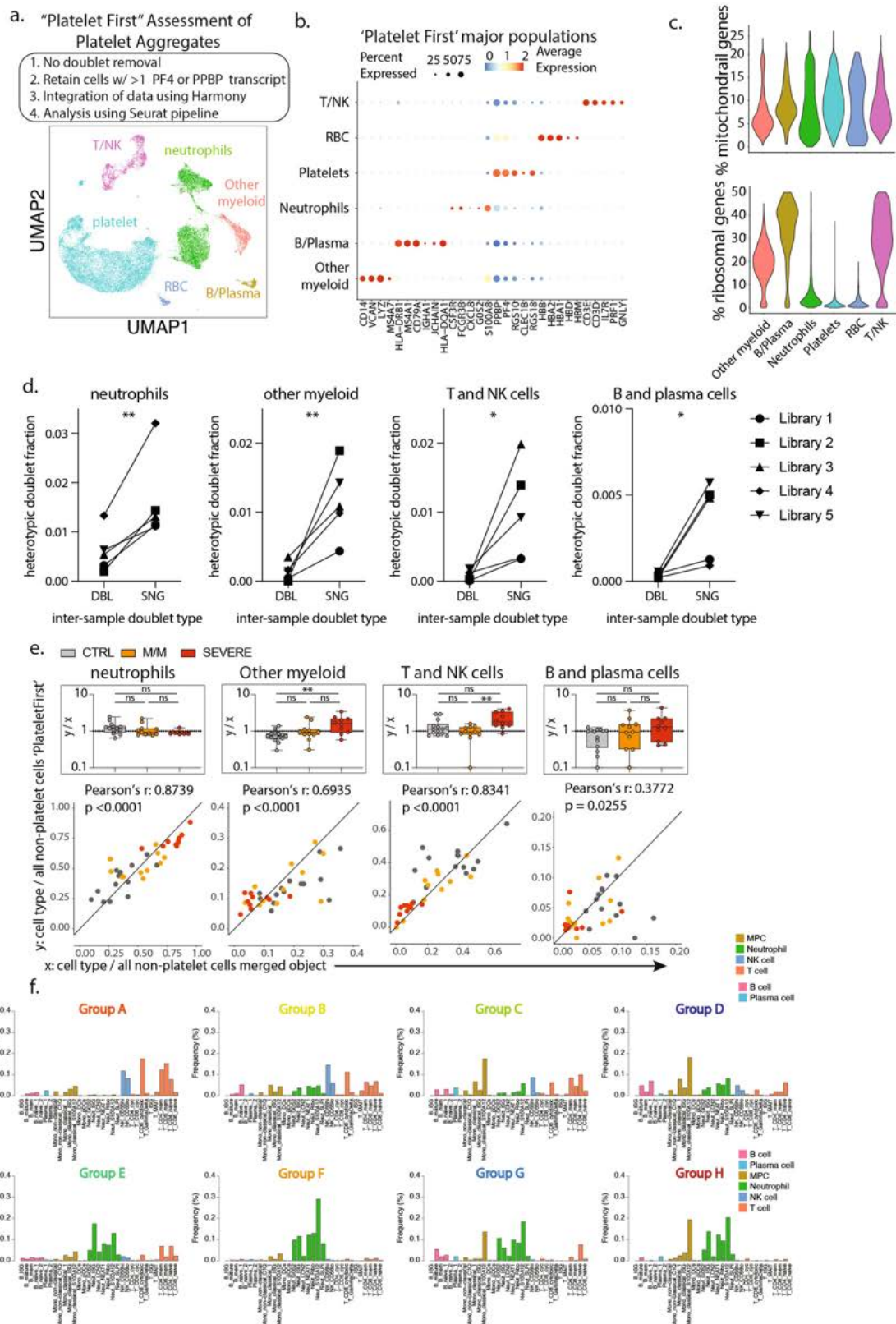
Extended Data Fig. 5 | Characterization of the subsets of peripheral blood T and B lymphocytes in our cohort. **a**, Dot plot of the top DEGs between clusters identified in the T and NK cell subset. **b**, UMAP visualization of 16,708 T and NK cells isolated from the entire dataset, showing various subsets, coloured by their identity. **c**, Overlay of the UMAP in **b** of all T and NK cells, coloured by disease severity, underlining the lack of batch effects that were present when merging the datasets from all patients. **d**, Abundance of the ISG⁺ subset among all T and NK cells in healthy control individuals ($n = 13$), patients who were negative for SARS-CoV-2 ($n = 9$) and patients who were positive for SARS-CoV-2 ($n = 15$) (top); and in healthy control individuals, patients with mild-moderate disease ($n = 14$) and patients with severe disease ($n = 9$) (bottom). **e**, ISG-signature score among healthy control individuals, patients who were negative

for SARS-CoV-2 and patients who were positive for SARS-CoV-2. **f**, Dot plot of the top DEGs between clusters identified in the B and plasma cell subset. **g**, UMAP visualization of 4,380 B and plasma cells isolated from the entire dataset, showing various subsets, coloured by their identity. **h**, Violin plots of canonical genes previously found to be expressed by B and plasma cells for each identified cluster. **i**, Frequencies of the identified clusters among all B and plasma cells in healthy control individuals ($n = 14$) and patients with patients with mild-moderate disease ($n = 17$) and patients with severe disease ($n = 15$). Statistical significance was assessed using a Kruskal-Wallis test (**d**, **e**) or a two-way ANOVA with multiple comparisons (**i**). * $P < 0.05$, ** $P < 0.01$, *** $P < 0.001$, **** $P < 0.0001$, NS, not significant. For box plots: centre line, median; box limits, 25th and 75th percentiles; whiskers, minimum and maximum values.



Extended Data Fig. 6 | Characterization of the subsets of peripheral blood platelets in our cohort. **a.** Dot plot of the top DEGs between clusters identified in the platelet subset. **b.** UMAP visualization of 16,903 platelets isolated from the entire dataset, showing various subsets, coloured by their identity. **c.** Frequencies of the identified clusters among all platelets in healthy control individuals ($n=14$) and in all patients with mild-moderate disease ($n=17$) and severe disease ($n=15$). **d.** UMAP visualization of all platelets coloured by *BCL2L1* (top) and violin plot of *BCL2L1* expression level across all identified platelet subsets. **e.** Violin plots of genes identifying young, reticulated platelets⁹ in the

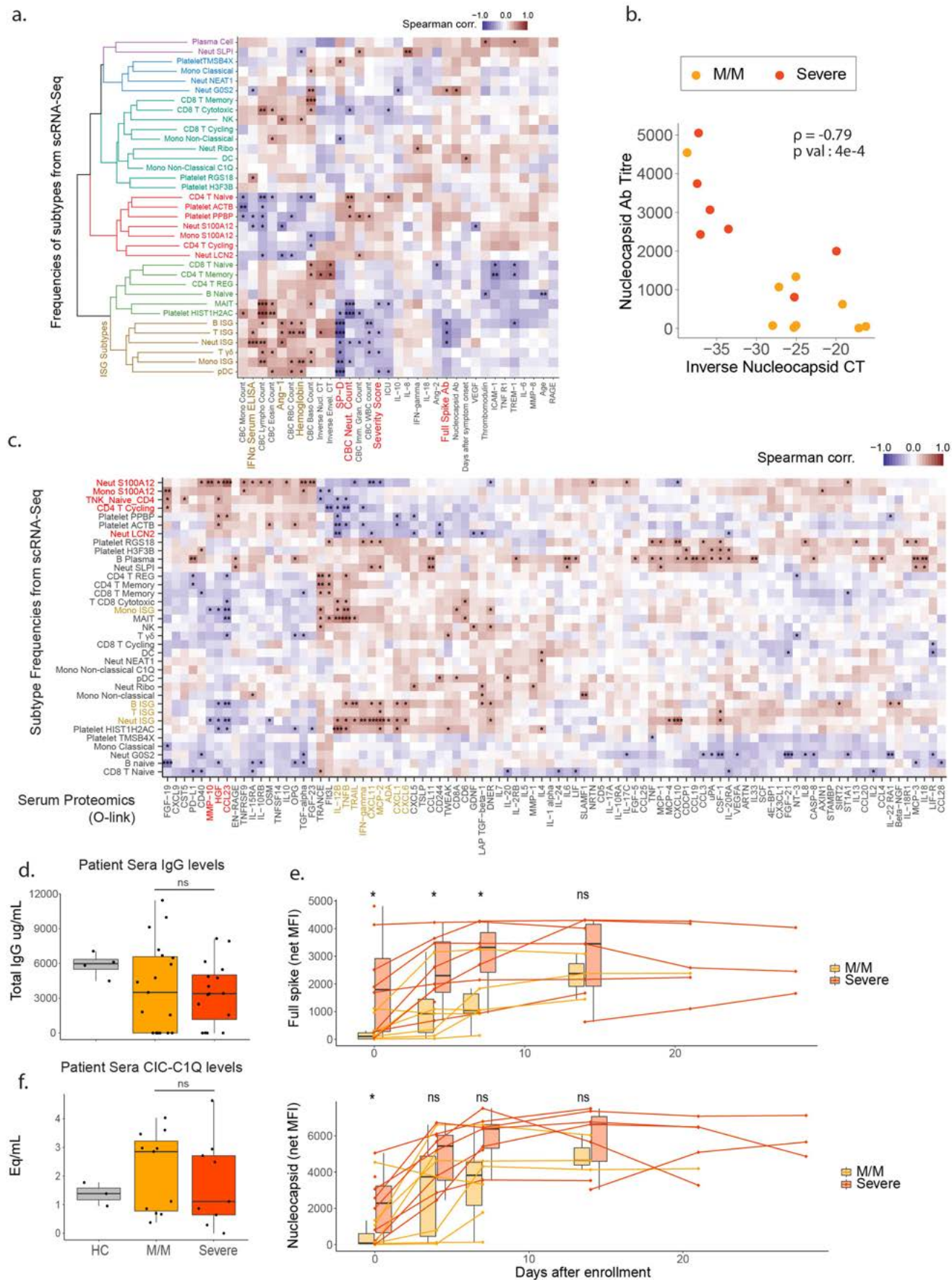
platelet dataset. **f.** UMAP visualization of all platelets with overlay of pseudotime trajectory. **g.** Violin plots of the relative pseudotime of each platelet cell subset present in **a**. **h.** Violin plot of the relative pseudotime of all platelets, split by disease severity. **i.** UMAP visualization of all platelets, coloured by ISG score. Statistical significance was assessed using a two-way ANOVA with multiple comparisons. * $P < 0.05$, ** $P < 0.01$, *** $P < 0.001$, **** $P < 0.0001$, NS, not significant. For box plots: centre line, median; box limits, 25th and 75th percentiles; whiskers, minimum and maximum values.



Extended Data Fig. 7 | See next page for caption.

Extended Data Fig. 7 | Leveraging scRNA-seq to assess platelet aggregates and define immune states in patients with COVID-19. **a**, Outline of 'platelet first' assessment to identify platelet aggregates in the entire whole-blood scRNA-seq dataset. UMAP visualization of the 52,757 putative platelet aggregates with specific populations overlaid. In this object no doublet-removal filtering step was applied to include all heterotypic cell-cell aggregates (step 1). This was followed by retaining all cells with more than one platelet-specific transcript PF4 or PPBP (step 2). Step 2 guaranteed analysis of cell events and aggregates containing platelets. As with our original dataset in Fig. 1b, integration of data was done using Harmony (step 3), and the 'platelet first' object was then analysed using the Seurat v.3 pipeline (step 4). **b**, Dot plot representation of the top DEGs between clusters identified in the 'platelet first' object. **c**, Violin plots of the percentages of mitochondrial and ribosomal genes within clusters identified in the 'platelet first' object. **d**, Inter-sample doublet rates in inferred platelet-involved heterotypic doublets show that platelet aggregates occur in vivo. DBL, doublet, $n = 5$ libraries. SNG, singlet, $n = 5$

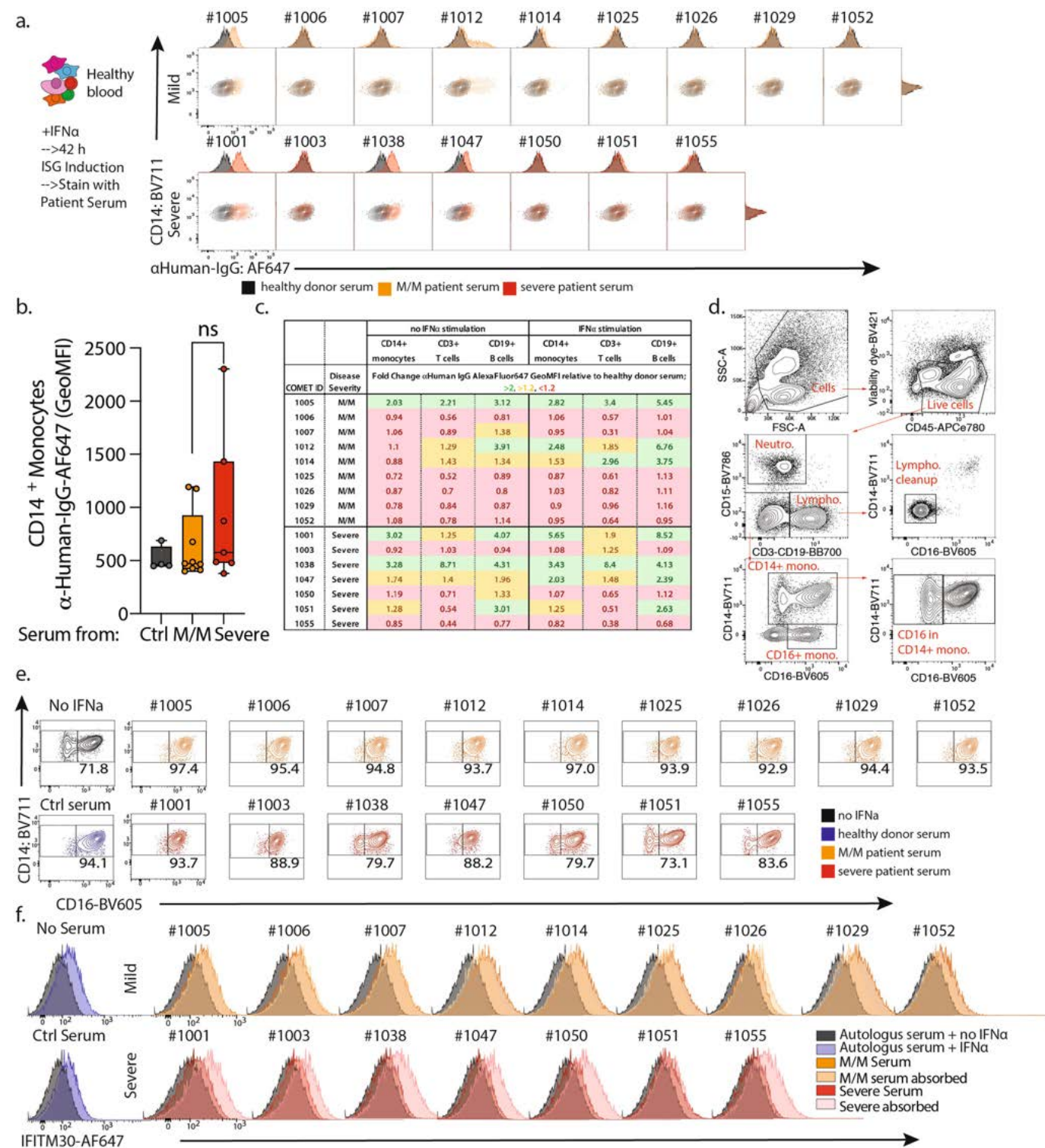
libraries. **e**, Bottom, scatter plots of cell-type frequency within merged object of entire cohort shown in Fig. 1b (x axis) versus same cell-type frequency within 'platelet first' object (y axis). The identity line $x = y$ is drawn as a reference. Each dot represents a sample from a healthy control individual ($n = 14$) or a sample from a patient who was positive for SARS-CoV-2, and dots are colour-coded by disease severity (M/M, $n = 11$; severe, $n = 10$). The Pearson's r correlation coefficient and two-tailed P value are shown for each cell type. Top, box plots of y/x ratio for each healthy control or patient sample, separated by disease severity. **f**, Cell fraction histograms representing bin-wise mean of relative frequency (that is, cell fraction) of each immune cell subtype for all patients in a given group, coloured as described in Fig. 2f. Statistical significance in **e** was assessed using a one-sided Student's t -test (**d**) or two-way ANOVA with multiple comparisons (**e**). * $P < 0.05$, ** $P < 0.01$, *** $P < 0.001$, **** $P < 0.0001$, NS, not significant. For box plots: centre line, median; box limits, 25th and 75th percentiles; whiskers, minimum and maximum values.



Extended Data Fig. 8 | See next page for caption.

Extended Data Fig. 8 | Holistic assessment of peripheral blood profiles from patients with COVID-19, combining scRNA-seq, clinical blood counts and plasma cytokine levels. **a**, Matrix of Spearman correlation coefficients between all subtype frequencies (out of major cell types; for example, ISG⁺ neutrophils out of all neutrophils) obtained from scRNA-seq versus patient metadata, viral load, antibody titres and serum analyte levels on a patient-by-patient basis excluding healthy control individuals. Patients for whom data were unavailable were excluded from correlation analysis for each comparison. Variables on both axes were ordered by hierarchical clustering with the computed dendrogram displayed for subtype frequencies. This dendrogram was divided into six groupings, with the one containing ISG⁺ subtypes highlighted in brown. Clinical variables that were generally correlated with severity are highlighted in red; those that were generally anticorrelated with severity are highlighted in brown (*n* for correlation comparisons ranged from *n* = 14–32 individuals). **P* < 0.05, ***P* < 0.005, ****P* < 0.0005. **b**, Scatter plots showing viral load versus levels of antibody binding the SARS-CoV-2 nucleocapsid protein for patients in the cohort of patients who were positive for SARS-CoV-2, with severity overlaid. Antibody levels are shown as arbitrary units of MFI from a Luminex assay; viral load is represented by an inverse *C_t* number from qRT-PCR with target amplification of the SARS-CoV-2 nucleocapsid sequence. Correlation coefficient and significance were calculated using Spearman's method. Patients for whom data was unavailable were excluded (M/M, *n* = 9; severe, *n* = 7 patients). **c**, Matrix of Spearman

correlation coefficients between all subtype frequencies (out of major cell types; for example, ISG⁺ neutrophils as a percentage of all neutrophils) obtained from scRNA-seq versus protein analyte abundance in plasma as measured using an Olink assay on a patient-by-patient basis excluding healthy control individuals. Patients for whom data were unavailable were excluded from correlation analysis for each comparison. Variables on both axes were ordered by hierarchical clustering. ISG⁺ subtypes and proteins that were strongly correlated with their frequency are highlighted in brown; subtypes and proteins that were strongly anticorrelated with ISG⁺ subtypes are highlighted in red (*n* = 31 for all comparisons). **P* < 0.05, ***P* < 0.005, ****P* < 0.0005. **d**, Computed total IgG levels in patient sera from ELISA absorbance readings. (*n* = 4, 19 and 16 for control, MM and severe, respectively). **e**, Longitudinal measurements of anti-spike and anti-nucleocapsid antibody levels in patient sera at the indicated days after enrolment in study. Connected points represent tracking of a single individual. (*n* = 11/8, 7/8, 6/7, 3/7, 1/5 and 0/3 for MM/severe for day 0, 4, 7, 14, 21 and 27, respectively). **f**, Levels of circulating immune complexes (CICs) in patient sera as measured by ELISA with human CIQ used to capture CICs and an anti-human IgG secondary antibody. Levels are shown as heat-aggregated human gamma globulin equivalents per ml (eq/ml) (*n* = 3, 11 and 9 for control, M/M and severe, respectively). Statistical significance was assessed using a two-sided Wilcoxon test. For box plots: centre line, median; box limits, 25th and 75th percentiles; whiskers, minimum and maximum values.

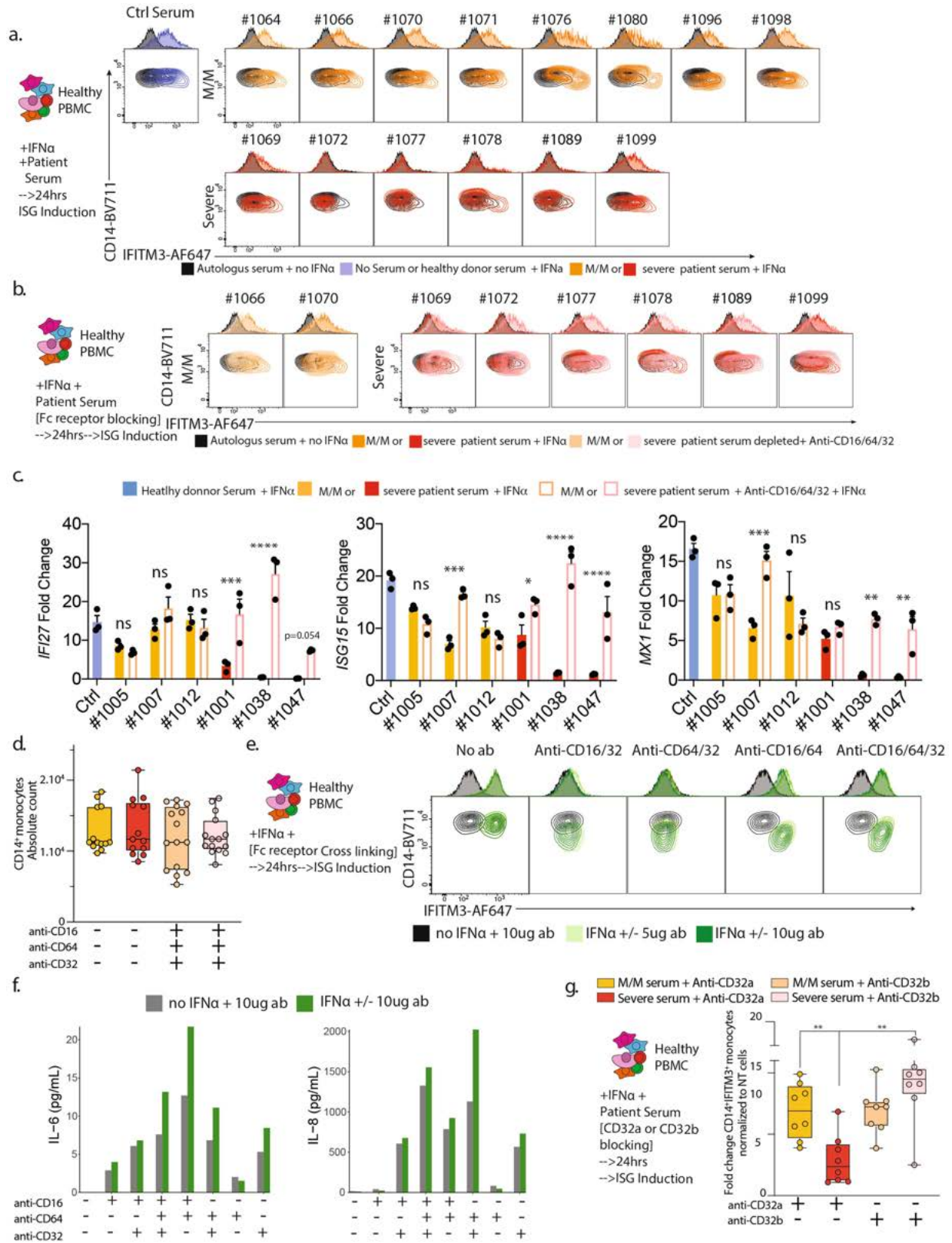


Extended Data Fig. 9 | See next page for caption.

Extended Data Fig. 9 | Staining and neutralization assay on interferon-stimulated healthy PBMCs using serum from patients with COVID-19.

a, Contour plots and histograms of CD14⁺ monocytes from healthy donor blood cultured with IFN α to induce expression of ISGs and stained with serum from healthy donors or from patients with mild–moderate or severe COVID-19, with secondary staining with anti-human IgG. **b**, Geometric MFI of serum staining on CD14⁺ monocytes treated with IFN α , quantifying data in **a** (control, $n = 4$; M/M, $n = 9$; severe, $n = 7$). Centre line, median; box limits, 25th and 75th percentiles; whiskers, minimum and maximum values. **c**, Summary table of serum staining experiment. The fold change in anti-human IgG–AlexaFluor647 geometric MFI relative to allogeneic healthy donor serum in nonstimulated and IFN α -stimulated healthy PBMCs is listed for each analysed cell type. Table data cells are colour-coded on the basis of degree of fold change; green, fold change > 2;

yellow, 2 > fold change > 1.2; red, fold change < 1.2. **d**, Gating strategy for PBMCs to identify different subpopulations. **e**, Modulation of the transition from intermediate to classical CD14 monocytes by serum from patients with mild–moderate (orange) and severe (red) COVID-19. Each plot represents a single serum sample. Representative experiment from three independent trials and two different healthy PBMC donors. **f**, IFITM3 expression by CD3⁺CD19⁺ lymphocytes from healthy donors, cultured with IFN α and serum from healthy donors (blue) or from patients with mild–moderate (orange) or severe (red) COVID-19. Mild–moderate (light yellow) and severe (pink) sera were pretreated with protein A/G before incubation with PBMCs. Each plot represents a single serum sample. Representative experiment from two independent trials and two different healthy PBMC donors. For **a–c**, **e**, **f**, data from one of two representative experiments are shown. NS, non-significant.



Extended Data Fig. 10 | See next page for caption.

Extended Data Fig. 10 | Antibodies present in patients with severe COVID-19 antagonize IFNAR signalling through FCγRIIb. **a**, Test of ISG neutralization by serum from patients with mild–moderate or severe COVID-19 as presented in Fig. 3e, here using sera from a validation cohort of patients. **b**, Test of ISG neutralization by serum from patients with mild–moderate or severe disease in the presence of anti-CD16, anti-CD64 and anti-CD32 antibodies to block Fc receptors as presented in Fig. 4a, here using sera from a validation cohort of patients. **c**, qPCR analysis of *IFI27*, *ISG15* and *MX1* gene expression in healthy donor PBMCs treated with IFNα with the addition of serum from patients with mild–moderate or severe disease, with or without Fc receptor blocking (Fig. 4a). Fold changes are relative to untreated healthy

donor PBMCs. $n = 3$ per group. Data are mean \pm s.e.m. **d**, Absolute counts of CD14⁺ monocytes from experiments presented in Fig. 4a ($n = 16$ per group). **e**, **f**, Contour plots and histograms of CD14 and IFITM3 expression by monocytes (**e**) and quantification by Luminex of IL-6 and IL-8 in the supernatant (**f**) from the experiments presented in Fig. 4b. **c**, **g**, Fold change in the percentage of IFITM3⁺CD14⁺ monocytes after IFNα stimulation, normalized to untreated cells (one experiment on two different PBMC donors; $n = 8$ per group). Statistical significance in **c**, **g** was assessed using a two-way ANOVA with multiple comparisons. * $P < 0.05$, ** $P < 0.01$, *** $P < 0.001$, **** $P < 0.0001$, NS, not significant. For box plots: centre line, median; box limits, 25th and 75th percentiles; whiskers, minimum and maximum values.

Reporting Summary

Nature Research wishes to improve the reproducibility of the work that we publish. This form provides structure for consistency and transparency in reporting. For further information on Nature Research policies, see our [Editorial Policies](#) and the [Editorial Policy Checklist](#).

Statistics

For all statistical analyses, confirm that the following items are present in the figure legend, table legend, main text, or Methods section.

n/a Confirmed

- ☐ ☒ The exact sample size (n) for each experimental group/condition, given as a discrete number and unit of measurement
- ☐ ☒ A statement on whether measurements were taken from distinct samples or whether the same sample was measured repeatedly
- ☐ ☒ The statistical test(s) used AND whether they are one- or two-sided
Only common tests should be described solely by name; describe more complex techniques in the Methods section.
- ☐ ☒ A description of all covariates tested
- ☐ ☒ A description of any assumptions or corrections, such as tests of normality and adjustment for multiple comparisons
- ☐ ☒ A full description of the statistical parameters including central tendency (e.g. means) or other basic estimates (e.g. regression coefficient) AND variation (e.g. standard deviation) or associated estimates of uncertainty (e.g. confidence intervals)
- ☐ ☒ For null hypothesis testing, the test statistic (e.g. F , t , r) with confidence intervals, effect sizes, degrees of freedom and P value noted
Give P values as exact values whenever suitable.
- ☒ ☐ For Bayesian analysis, information on the choice of priors and Markov chain Monte Carlo settings
- ☒ ☐ For hierarchical and complex designs, identification of the appropriate level for tests and full reporting of outcomes
- ☐ ☒ Estimates of effect sizes (e.g. Cohen's d , Pearson's r), indicating how they were calculated

Our web collection on [statistics for biologists](#) contains articles on many of the points above.

Software and code

Policy information about [availability of computer code](#)

Data collection FacsDiva used for collecting flow cytometry data

Data analysis R code used for scRNA-Seq analysis uploaded to Github link at: https://github.com/UCSF-DSCOLAB/combes_et_al_COVID_2020
Seurat v3 used for analysis
Monocle v3 used for analysis
FlowJo v10
Statistical analyses performed in R and GraphPad Prism v9

For manuscripts utilizing custom algorithms or software that are central to the research but not yet described in published literature, software must be made available to editors and reviewers. We strongly encourage code deposition in a community repository (e.g. GitHub). See the Nature Research [guidelines for submitting code & software](#) for further information.

Data

Policy information about [availability of data](#)

All manuscripts must include a [data availability statement](#). This statement should provide the following information, where applicable:

- Accession codes, unique identifiers, or web links for publicly available datasets
- A list of figures that have associated raw data
- A description of any restrictions on data availability

Due to the size of our dataset (~1.3Terabytes) we were unable to submit our data to GEO directly in the timespan between being accepted in principle, and final revision. We are working with GEO and SRA to deposit our data and link them into GEO accessions. We include the following statement:

"Cellranger-processed raw feature-barcode matrices are available at GEO using accession GSE163668 and raw fastq files for all 10X libraries are deposited in SRA. Scripts used to process all data along with relevant clinical information for each patient are available at https://github.com/UCSF-DSCOLAB/combes_et_al_COVID_2020."

Field-specific reporting

Please select the one below that is the best fit for your research. If you are not sure, read the appropriate sections before making your selection.

☒ Life sciences ☐ Behavioural & social sciences ☐ Ecological, evolutionary & environmental sciences

For a reference copy of the document with all sections, see [nature.com/documents/nr-reporting-summary-flat.pdf](https://www.nature.com/documents/nr-reporting-summary-flat.pdf)

Life sciences study design

All studies must disclose on these points even when the disclosure is negative.

Sample size	Our goal was to compare the immune profile of SARS-CoV-2 infected patients with the one of non SARS-CoV-2 infected individuals presenting with pulmonary infection and with the one of control individuals. Among the sick patients we also wanted to compare disease severity and we thus aimed at recruiting at least 5 patients in each of the 4 disease groups. We thus prospectively enrolled 40 patient without knowing their infectious status nor disease severity in order to ensure the study of at least 5 patient per group after screening and removal of patients who waived their consent. We tried to move rapidly with patient enrollment due to the urgency of the COVID-19 pandemic and we determined this to be the minimum necessary # of patients.
Data exclusions	We excluded all the data from the patients who waived their consent between sample collection and manuscript submission.
Replication	Sequencing of patients' cells happened over the course of 1 month, thus describing multiple technical batches generated by different individuals. Our analyses are based on the merging of these multiple datasets after batch correction, thus avoiding potential technical biases. Serum skewing experiments were replicated at least once successfully.
Randomization	Patients were assigned to our experimental groups according to the examination of their SARS-CoV-2 tests and of their clinical parameters, as described in the methods. Our study focuses on these experimental groups and asks if they are linked to any immunological profile in the blood, for that reason our patients cannot be randomized. Nevertheless we examined covariates Age, Sex and Race and found no significant skewing of these variables in our mild/moderate and severe categories and Covid +/-.
Blinding	Patients were prospectively enrolled in our study and the investigators remained blind to their clinical features until final analyses. The determination of M/M and severe clinical criteria was done prior to analysis of immune cell profiles. Serum assays were originally performed blindly by the investigators without knowing the severity status of the corresponding patients.

Reporting for specific materials, systems and methods

We require information from authors about some types of materials, experimental systems and methods used in many studies. Here, indicate whether each material, system or method listed is relevant to your study. If you are not sure if a list item applies to your research, read the appropriate section before selecting a response.

Materials & experimental systems

n/a	Involved in the study
<input type="checkbox"/>	<input checked="" type="checkbox"/> Antibodies
<input checked="" type="checkbox"/>	<input type="checkbox"/> Eukaryotic cell lines
<input checked="" type="checkbox"/>	<input type="checkbox"/> Palaeontology and archaeology
<input checked="" type="checkbox"/>	<input type="checkbox"/> Animals and other organisms
<input type="checkbox"/>	<input checked="" type="checkbox"/> Human research participants
<input checked="" type="checkbox"/>	<input type="checkbox"/> Clinical data
<input checked="" type="checkbox"/>	<input type="checkbox"/> Dual use research of concern

Methods

n/a	Involved in the study
<input checked="" type="checkbox"/>	<input type="checkbox"/> ChIP-seq
<input type="checkbox"/>	<input checked="" type="checkbox"/> Flow cytometry
<input checked="" type="checkbox"/>	<input type="checkbox"/> MRI-based neuroimaging

Antibodies

Antibodies used	Unconjugated AffiniPure Fab Fragment Goat anti-human IgG (H+L) (Jackson ImmunoResearch; #109-007-003), TruStain FcX block (BioLegend; #422302), AffiniPure Donkey anti-human IgG-Alexa Fluor 647 antibody (Jackson ImmunoResearch; #709-605-149), anti-human CD3-BB700 (clone SK7; BD Biosciences; #566575), anti-human CD14-BV711 (clone MSE2; BioLegend; #301838), anti-human CD15-BV786 (clone W6D3; BD Biosciences; #741013), anti-human CD16-BV605 (clone 3G8; BioLegend; #302040), anti-human CD19-BB700 (clone SJ25C1; BD Biosciences; 566396), anti-human CD45-APCeFluor780 (clone HI30; ThermoFisher; 47-0459-42), anti-human IFITM3-AlexaFluor 647 (clone EPR5242; Abcam; ab198573). For Fc blocking and cross-linking: Anti-CD16 (3G8 from Biolegend), anti-CD32 (FUN-2 Biolegend), anti-64 (10.1 Biolegend), anti-CD32a (Clone IV.4 BioXCell), and anti-CD32b/c (S18005H Biolegend)
Validation	All antibodies were validated by their respective manufacturers and individually tested and titrated on relevant positive and negative

Validation

biological controls by the investigators.
 Abcam IFITM3-AF647 validated by imaging.
 BD antibodies validated by flow cytometry.
 Jackson Immunology antibodies validated by ELISA
 All biolegend antibodies validated through flow cytometry.
 ThermoFisher antibody validated by flow cytometry

Human research participants

Policy information about [studies involving human research participants](#)

Population characteristics

These informations are listed in our supplementary table 1 describing age, sex and race of enrolled individuals

Recruitment

Patients admitted to the Hospital of the University of California with known or presumptive COVID-19 were screened within 3 days of hospitalization. Patients, or a designated surrogate, provided informed consent to participate in the study. This study includes a subset of patients enrolled between April 8 and May 1 in the COMET (COVID-19 Multi-immunophenotyping projects for Effective Therapies; <https://www.comet-study.org/>) study at UCSF. Healthy donors were adults with no prior diagnosis of or recent symptoms consistent with COVID-19. This analysis includes samples from participants who provided informed consent directly, via a surrogate, or otherwise in accordance with protocols approved by the regional ethical research boards and the Declaration of Helsinki. For inpatients, clinical data were abstracted from the electronic medical record into standardized case report forms. Potential biases include: patients enrolled were early in the pandemic and dependent on patients reporting to the hospital, and restricted to the greater Bay Area of California.

Ethics oversight

This study is approved by the Institutional Review board: UCSF Human Research Protection Program (HRPP) IRB# 20-30497.

Note that full information on the approval of the study protocol must also be provided in the manuscript.

Flow Cytometry

Plots

Confirm that:

- ☒ The axis labels state the marker and fluorochrome used (e.g. CD4-FITC).
- ☒ The axis scales are clearly visible. Include numbers along axes only for bottom left plot of group (a 'group' is an analysis of identical markers).
- ☒ All plots are contour plots with outliers or pseudocolor plots.
- ☒ A numerical value for number of cells or percentage (with statistics) is provided.

Methodology

Sample preparation

Sample preparation is extensively described in our manuscript in the methods section.

Instrument

Fortessa X-20, BD.

Software

Acquisition of flow cytometry data was done using BD FACSDiva version 8.01, and analysis using BD FlowJo version 10.7.1

Cell population abundance

No sorting was used in this study.

Gating strategy

Presented in Figure S7A:
 Cells were gated according to their FSC/SSC profile
 Live cells were gated according to their negative signal in the Live/dead channel
 Neutrophils were gated as CD15+
 Lymphocytes were gated as CD3/CD19+ (both markers have been put in the same channel) CD14-CD16-
 CD14+ monocytes were gated as CD15-CD3/19-CD14+CD16+/-
 CD16+ monocytes were gated as CD15-CD3/19-CD14-CD16+

- ☒ Tick this box to confirm that a figure exemplifying the gating strategy is provided in the Supplementary Information.